

1 **The oxygen sensor Prolyl hydroxylase domain 2 regulates**
2 **the in vivo suppressive capacity of regulatory T cells**

3
4
5 Yousra Ajouaou^{1,2}, Abdulkader Azouz^{1,3}, Anaelle Taquin^{1,2}, Sebastien
6 Denanglaire^{1,2}, Hind Hussein^{1,2}, Mohammad Krayem^{4,5}, Fabienne Andris^{1,2},
7 Muriel Moser^{1,2}, Stanislas Goriely^{1,2,3} and Oberdan Leo^{1,2*}

8
9
10 ¹U-CRI (ULB Center for Research in Immunology), Université Libre de Bruxelles (ULB),
11 Gosselies, Belgium,

12 ²Immunobiology laboratory, Université Libre de Bruxelles (ULB), Gosselies, Belgium,

13 ³Institute for Medical Immunology, Université Libre de Bruxelles (ULB), Gosselies, Belgium,

14 ⁴Department of Radiation Oncology, Institut Jules Bordet, Université Libre de Bruxelles,
15 Brussels, Belgium,

16 ⁵Laboratory of Clinical and Experimental Oncology (LOCE), Institut Jules Bordet, Université
17 Libre de Bruxelles, Brussels, Belgium.

18
19
20 *Corresponding author: Oberdan Leo (Oberdan.Leo@ulb.be), Immunobiology laboratory, IBMM,
21 Rue des Professeurs Jeener et Brachet 12, 6041 Gosselies (Belgium).

24 **Abstract**

25 The oxygen sensor PHD2 (prolyl hydroxylase domain 2) plays an important role in cell
26 hypoxia adaptation by regulating the stability of HIF proteins (HIF1 α and HIF2 α) in
27 numerous cell types including T lymphocytes. The role of oxygen sensor on immune
28 cells, in particular on regulatory T cell (Treg) function, has not been fully elucidated. The
29 purpose of our study was to evaluate the role of PHD2 in the regulation of Treg
30 phenotype and function. We demonstrate herein that selective ablation of PHD2
31 expression in Treg (PHD2 Δ^{Treg} mice) leads to a spontaneous systemic inflammatory
32 syndrome, as evidenced by weight loss, development of a rectal prolapse,
33 splenomegaly, shortening of the colon and elevated expression of IFN- γ in the
34 mesenteric lymph nodes, intestine and spleen. PHD2 deficiency in Tregs led to an
35 increased number of activated CD4 conventional T cells expressing a Th1-like effector
36 phenotype. Concomitantly, the expression of innate-type cytokines such as *Il1b*, *Il12a*,
37 *Il12b* and *Tnfa* was found to be elevated in peripheral (gut) tissues and spleen.
38 PHD2 Δ^{Treg} mice also displayed an enhanced sensitivity to DSS-induced colitis and to
39 toxoplasmosis, suggesting that PHD2-deficient Tregs did not efficiently control
40 inflammatory response in vivo, in particular those characterized by IFN- γ production.
41 Further analysis revealed that Treg dysregulation was largely prevented in PHD2-HIF2 α
42 (PHD2-HIF2 $\alpha^{\Delta^{\text{Treg}}}$ mice), but not in PHD2-HIF1 α (PHD2-HIF1 $\alpha^{\Delta^{\text{Treg}}}$ mice) double KOs,
43 suggesting an important and possibly selective role of the PHD2-HIF2 α axis in the
44 control of Treg function. Finally, the transcriptomic analysis of PHD2-deficient Tregs
45 identified the STAT1 pathway as a target of the PHD2-HIF2 α axis in regulatory T cell
46 phenotype and in vivo function.

47

48 Key words: Regulatory T cells/ Oxygen sensor/ Hypoxia inducible factor/ Inflammation

49 Introduction

50 CD4⁺ regulatory T cells (Tregs), accounting for approximately 5-10% of total
51 circulating CD4⁺ T cells, represent a critical subset of T lymphocytes involved in immune
52 homeostasis. Through a broad set of effector mechanisms, these cells contribute to
53 immune tolerance to self-constituents and to mucosal antigens derived from the
54 commensal microflora and food^{1,2}. Tregs also participate in the resolution of
55 inflammatory responses³ and play an important role in maternal immunotolerance
56 against the semi-allogeneic fetus⁴. While critical to maintain tissue integrity, excessive
57 activation of Tregs impedes adequate immune responses to tumors and pathogens,
58 suggesting a tight control of their suppressive activity and tissue localization⁵⁻⁷. Although
59 uniformly characterized by the expression of the lineage-specific, Foxp3 transcription
60 factor¹, regulatory T cells display a wide range of phenotypic and functional properties
61 that allow them to migrate to specific sites and suppress a variety of immune reactions
62 including inflammatory⁸ and humoral responses⁹. Although diverse, the mechanisms
63 whereby Tregs antagonize the activity of immune effectors are largely paracrine in
64 nature¹⁰. Short-range suppressive mechanisms include competition for nutrients and/or
65 growth factors (mostly cytokines), secretion of immunosuppressive factors and direct,
66 contact-mediated, inactivation of antigen presenting cells¹¹. These findings suggest that
67 Tregs have to adapt to multiple lymphoid and non-lymphoid environments and suppress
68 immune responses in a context and tissue-dependent fashion^{12,13}.

69 Oxygen represents an essential component of cellular bioenergetics and
70 biochemistry. Because oxygen tension varies according to tissues and
71 pathophysiological states¹⁴, cells need to adapt to fluctuations in oxygen availability in
72 order to maintain an adequate functional and metabolic status. Of note, low oxygen
73 availability (hypoxia) plays a critical role in the pathophysiology of many immune
74 disorders^{15,16}. Inflammation, in particular, is thought to reduce oxygen availability to
75 tissues by affecting microvascular form and function, and through the recruitment of
76 highly oxygen consuming inflammatory cells producing NADPH oxidase-derived reactive
77 oxygen species¹⁷.

78 Immune cells patrolling through lymphoid and non-lymphoid tissues need therefore to
79 readily adapt to varying oxygen concentration levels in order to exert their function¹⁸,
80 suggesting an important role for oxygen sensors in immune regulation. Several hypoxia-
81 sensitive pathways are known to enable single cell survival in low oxygen settings. In
82 particular, reduced oxygen levels are directly sensed by a family of oxygen-dependent
83 prolyl hydroxylases (PHD encoded by *Egln* gene, comprising three members)¹⁹,
84 although other mechanisms mediated by oxygen-sensitive histone lysine demethylases
85 (KDM) and the cysteamine dioxygenase/N-degron pathway have been recently
86 uncovered²⁰. Hypoxia-inducible factors (HIFs), a set of evolutionary conserved

87 transcriptional regulators, represent the best-described substrates of PHDs. These
88 factors are heterodimers composed of a HIF α subunit whose stability is directly
89 controlled by oxygen availability, and a constitutively expressed HIF1 β subunit (also
90 known as ARNT)²¹. Following the initial characterization of the first member of HIF α
91 family (HIF1 α), two additional members, HIF2 α and HIF3 α have been identified and
92 shown to be similarly regulated by O₂ availability and to bind to HIF1 β ²². In normoxia,
93 PHDs, whose affinity for oxygen is low and comparable to atmospheric concentrations,
94 catalyze the prolyl-hydroxylation of HIF α subunits²³. This post-translational modification
95 allows recognition and ubiquitination of HIF α subunits by the E3 ubiquitin ligase Von
96 Hippel-Lindau protein (pVHL) and subsequent degradation by the proteasome²⁴. In
97 hypoxia, non-hydroxylated alpha subunits escape degradation, and translocate to the
98 nucleus where they bind to constitutively expressed and stable beta subunits to
99 constitute an active heterodimer able to regulate gene expression. This process
100 promotes transcriptional regulation of numerous genes ultimately leading to increased
101 oxygen supply (such as angiogenesis) and promotion of anaerobic metabolism²⁵.

102 Multiple levels of complexity of this major regulatory axis have been recently
103 uncovered. As previously suggested, the presence of several members of the PHD and
104 HIF families suggests specialized functions of PHD-HIF pairs during ontogeny and in
105 selected tissues²⁶. In particular, while HIF1 α appears as ubiquitously expressed in all
106 metazoans, HIF2 α represents a late acquisition of vertebrates, displaying a more
107 restricted tissue expression pattern²⁷. Although these factors bind to similar sequence
108 motifs (hypoxia response elements or HREs) and regulate the expression of a shared
109 set of genes, both HIF1 α and HIF2 α specific gene targets have been identified in
110 multiple tissues^{25,28,29}. Further complexity in this pathway stems from the possible
111 occurrence of additional, non-HIF-related, PHD substrates³⁰⁻³⁷, a set of findings that
112 however has not been confirmed in more rigorous in vitro settings using well defined
113 synthetic substrates³⁸.

114 Hypoxia plays a dual role in inflammation and in the regulation of immune responses.
115 In most settings, hypoxia promotes inflammation, while in some instances, such as in
116 tumor sites, low oxygen levels generally cause unresponsiveness of immune effectors,
117 thus favoring tumor growth. The often-opposing effects displayed by HIF activation on
118 the activity of immune cells equally match this complexity³⁹. Previous work has indeed
119 highlighted the important role of the PHD-HIF axis in regulating both innate and adaptive
120 immune effectors²⁶. The role of HIF1 α in regulating T cell activity has been described in
121 many studies, and mainly linked to the capacity of this hypoxia-induced transcription
122 factor to promote glycolysis (for a review see McGettrick & O'Neill⁴⁰). Accordingly, HIF1 α
123 expression favors the development of highly glycolytic inflammatory Th17 cells, while
124 inhibiting the development of Tregs which rely mostly on aerobic metabolism⁴¹. HIF1 α
125 also plays a direct role in Th17 development, through the transcriptional activation of

126 *Rorc*⁴². The role of HIF1 α in Th1 development appears as more complex, and context-
127 dependent. Hypoxia decreases IFN- γ production of Th1-like cells in a HIF1 α dependent
128 fashion⁴³, while sustained expression of this transcription factor in normoxia (as
129 observed in mice lacking PHDs expression⁴⁴) leads to an increase in IFN- γ secreting
130 CD4⁺ T cells. Of note, expression of HIF1 α can be upregulated in normoxia both by
131 TCR⁴⁵ and cytokine-initiated signals⁴², confirming that HIF1 α may play a role in Th1 cells
132 development both in hypoxia and normoxia.

133
134 The role of hypoxia-induced factors in Treg development and function is presently
135 not fully elucidated. As previously discussed, HIF1 α -deficiency improves Treg cell
136 development, possibly a consequence of the limited requirement for glycolysis of this
137 cell subset⁴¹. However, hypoxia promotes Foxp3 expression in a HIF1 α dependent
138 fashion⁴⁶ (and expression of HIF1 α is required for adequate regulatory T cell function⁴⁷).
139 Similarly, a recent report has identified HIF2 α as an important mediator of Treg function
140 in vivo, further stressing the important role of these hypoxia-induced factors in the
141 control of in vivo inflammatory manifestations⁴⁸. In agreement with these conclusions,
142 PHDs proteins have also been shown to play a role in the differentiation of peripheral
143 (but not thymic-derived) Tregs⁴⁴. Expression of these proteins appears to redundantly
144 regulate Th1 vs iTreg development, mostly by limiting the accumulation of HIF1 α . In
145 contrast to this study, a recent publication has highlighted a selective role of the PHD2
146 isoform in the regulation of Treg function⁴⁹. ShRNA mediated knockdown of PHD2
147 expression in Foxp3-expressing cells (PHD2-KD Tregs) led to a systemic inflammatory
148 syndrome characterized by mononuclear cell infiltration in several organs. PHD2-KD
149 Tregs displayed reduced suppressive capacities both in vitro and in vivo, suggesting an
150 important and intrinsic role of PHD2 in this cell subset. Of interest, loss of HIF2 α
151 expression reversed the phenotype of these mice bearing PHD2-KD Tregs, suggesting
152 an important role of the PHD2-HIF2 α axis in regulating Treg function.

153
154 To better delineate the role of PHD2, HIF1 α and HIF2 α in the regulation of Treg
155 development and function, we have generated a set of conditional mouse strains lacking
156 expression of these hypoxia responsive proteins in Foxp3⁺ cells. Using these tools, we
157 confirm herein that mice in which expression of PHD2 is selectively inactivated in
158 regulatory T cells display a spontaneous inflammatory syndrome characterized by
159 altered immune homeostasis at the steady-state and high sensitivity to Th1-type
160 inflammatory diseases. This proinflammatory phenotype was accentuated by the
161 concomitant loss of PHD2 and HIF1 α , but almost completely alleviated in mice dually
162 deficient for PHD2 and HIF2 α . Transcriptome analysis confirmed a marginal role for
163 HIF1 α -dependent enhanced glycolysis in the regulation of Treg function and allowed us
164 to identify STAT1 as a potential target of the PHD2-HIF2 α axis in maintaining immune
165 homeostasis and preventing excessive Th1-mediated inflammation.

166

167 **Results**

168 **Deletion of PHD2 in Tregs leads to a systemic, type-1-like, inflammatory syndrome**
169 **associated to altered Treg numbers and phenotype.**

170 Based on the predominance of *Egln1* (PHD2) expression in Tregs over other
171 members of the prolyl hydroxylases family, we generated a mouse strain lacking PHD2
172 expression in Tregs (identified as PHD2^{ΔTreg}) (**Figure 1 and Figure 1-figure**
173 **supplement 1**), as described in the Methods section. These mice displayed a strongly
174 reduced expression of *Egln1* mRNA in Tregs, while retaining control level expression of
175 this enzyme in other, non-Treg spleen and peripheral lymph node cells (**Figure 1-figure**
176 **supplement 1**). Upregulation of GLUT1 expression, a well-known target of HIF1α, was
177 also only found in Foxp3-expressing cells in these mice, further supporting the selective
178 depletion of PHD2 in Tregs vs T convs (**Figure 1-figure supplement 1**). While fertile
179 and viable, over 70% of these mice developed a spontaneous inflammatory syndrome,
180 characterized by weight loss, episodes of anal prolapse, reduced colon length,
181 splenomegaly and hemorrhagic abdomen (**Figure 1a-e**). This last feature is most likely
182 due to an increased blood hematocrit (with enhanced numbers of circulating red blood
183 cells) associated to an elevation in vascular permeability, as shown in **Figure 1-figure**
184 **supplement 2**. Although the frequency of CD4⁺ and CD8⁺ conventional T lymphocytes
185 (see **Figure 1-figure supplement 3** for gating strategy) in several lymphoid organs were
186 not significantly altered in PHD2^{ΔTreg} mice (**Figure 1f**), the total number of CD4⁺ cells
187 was increased in the peripheral lymphoid organs of these mice (**Figure 1-figure**
188 **supplement 4**). Moreover, these lymphocytes displayed clear signs of spontaneous
189 activation, as evidenced by the significant increase in the expression of markers (i.e
190 CD44) associated to an effector-like phenotype (**Figure 1g, h**). Confirming these
191 findings, intracellular staining of short-term stimulated T cells (using pharmacological
192 agents bypassing TCR signaling) revealed an increased capacity of conventional T cells
193 from PHD2^{ΔTreg} mice to produce IFN-γ, while retaining control-like production of IL-17
194 (**Figure 1i**). The ex-vivo evaluation of mRNA abundance in whole, unfractionated, mLNs
195 similarly showed a significantly elevated expression of type 1-associated adaptive and
196 innate cytokines including *Ifng*, *Il1b*, both *Il12* subunits and *Tnfa* (**Figure 1j**). Overall,
197 these observations point to the establishment of a Th1-like, pro-inflammatory
198 environment in mice possessing PHD2-deficient Tregs.

199 Much to our surprise, flow cytometric analysis of lymphoid organs from naive animals
200 revealed an increased frequency of Treg cells in the spleen, lymph nodes and lamina
201 propria of PHD2^{ΔTreg} mice, when compared to control animals (**Figure 2a**). To evaluate
202 the possible influence of PHD2 deletion on Treg development, thymic cell suspensions
203 were analyzed for the expression of early Treg markers including Foxp3, CD25 and

204 CD24⁵⁰. Recent studies have revealed that mature Foxp3^{high} CD25⁺ Tregs can
205 differentiate from two distinct thymic precursors identified as respectively CD25⁺ Foxp3⁻
206 and CD25⁻ Foxp3^{low} precursor Tregs (pre-Tregs). Analysis of thymic cell suspensions
207 revealed an accumulation of the Foxp3^{low} pre-Tregs and a reduction in the number of
208 mature Tregs in PHD2-deficient, Foxp3-expressing cells, suggesting an early role for
209 PHD2 in the generation of thymic-derived Tregs (**Figure 2b, c**). Accordingly, PHD2-
210 deficient, Foxp3-expressing cells retained higher expression of CD24 (**Figure 2d**), a
211 marker associated to a thymic immature state⁵⁰, further confirming a putative role for
212 PHD2 in the development of thymic-derived Tregs. No difference in the relative
213 frequency of Treg subsets identified by the co-expression of Foxp3 with either naive and
214 memory markers (**Figure 2e**) or with master transcription factors T-bet, GATA3 or
215 ROR γ t (**Figure 2f**) was noted in these mice. The phenotype of splenic, PHD2-deficient
216 Tregs was however significantly altered, showing a slight, but statistically significant
217 reduction in the expression of Foxp3 (**Figure 2g**), accompanied by reduced expression
218 of the CD25, ICOS, and CD44 markers and enhanced expression of PD-1 (**Figure 2h**).
219 Of note, neither CTLA-4 (**Figure 2h**) nor *Il10* (**Figure 2i**) expression was altered in
220 PHD2-deficient Tregs. To evaluate the functional consequences of PHD2-deletion on
221 peripheral Treg development, we generated Tregs from naive, conventional T cells using
222 a well-established in vitro protocol. In keeping with in vivo observations, culture of CD4⁺
223 T conv from PHD2^{ΔTreg} mice led to a consistently higher yield of Foxp3-expressing cells
224 when activated in the presence of Treg-inducing cytokines (**Figure 2j, k**). In contrast to
225 their in vivo counterparts, these induced Tregs displayed control level expression of
226 Foxp3 (**Figure 2l**).

227 To evaluate whether the altered phenotype of PHD2-deficient Tregs was a cell-
228 autonomous phenomenon, heterozygous *Foxp3*^{cre/+} *Egln1*^{fl/fl} mice in which both PHD2-
229 sufficient (YFP-negative) and PHD2-deficient (YFP-positive) Tregs co-exist were
230 examined (**Figure 3**). These mice did not display any sign of inflammation or
231 hematological dysfunction and were morphologically (cf weight, colon length and spleen
232 size) indistinguishable from *Foxp3*^{cre} or *Foxp3*^{cre/+} mice (this latter strain displaying the
233 expected 1:1 ratio of YFP-pos:YFP-neg cells). Surprisingly, WT Tregs outcompeted
234 PHD2-deficient Tregs in all compartments examined in *Foxp3*^{cre/+} *Egln1*^{fl/fl} mice (i.e.
235 thymus, spleen, and peripheral lymph nodes, **Figure 3a**). A similar trend was observed
236 following the transfer of an equal mix of WT and PHD2-deficient Tregs in *Rag2*-deficient
237 mice (data not shown), strongly suggesting that PHD2 expression plays a role in Treg
238 fitness and survival in the periphery. As previously shown in **Figure 2**, PHD2-deficient
239 Tregs expressed lower levels of Foxp3, CD25 and CD44, indicative of an intrinsic role of
240 PHD2 in regulating Treg phenotype (**Figure 3b-e**). However, expression of CTLA-4 was
241 not altered in PHD2-deficient Tregs (**Figure 3b, f**). Whether the altered fitness / capacity
242 to repopulate the periphery of PHD2-deficient Tregs is due to reduced expression of
243 CD25 remains to be established.

244 **In vivo reduced suppressive function of PHD2-deficient Tregs.**

245 To evaluate the suppressive capacity of PHD2-deficient Tregs cells, ex-vivo purified
246 CD45.2 expressing Tregs from control and PHD2^{ΔTreg} mice were adoptively co-
247 transferred into syngeneic Rag-deficient mice with CFSE-labelled, CD45.1-expressing
248 CD4⁺ naive T lymphocytes (**Figure 4a**). In the absence of Tregs, transferred naive cells
249 rapidly divided and acquired an effector-like phenotype, a well-established consequence
250 of homeostatic proliferation in a lymphopenic environment (**Figure 4b**). Addition of WT
251 Tregs in the inoculum led to a significant reduction of conventional T cell proliferation
252 and phenotype switch, while PHD2-deficient Tregs appeared functionally impaired in this
253 assay (**Figure 4b-d**). Lack of suppressive activity of these Tregs was not a consequence
254 of reduced viability and/or in vivo survival, as shown by the normal recovery rate of both
255 Treg-populations at the time of assay read-out (**Figure 4e**). In contrast, when tested in
256 vitro, PHD2-deficient Tregs consistently displayed a fully functional suppressive activity
257 (**Figure 4f, g**).

258 259 **Increased susceptibility of PHD2^{ΔTreg} mice to type-1 experimental inflammation**

260 A series of experimental acute and chronic inflammatory models were employed to
261 further evaluate the capacity of PHD2^{ΔTreg} mice to sustain an in vivo inflammatory
262 challenge. We first exposed mice to a chemical-induced colitis protocol. This assay
263 revealed an increased sensitivity of PHD2^{ΔTreg} mice to most DSS-induced inflammatory
264 manifestations, including weight loss (**Figure 5a**), survival (**Figure 5b**), clinical score
265 (**Figure 5c**) and colon length (**Figure 5d**). No difference was noted however in crypt
266 morphology induced by DSS in both mouse strains (**Figure 5e**). Similar observations
267 were made when mice were acutely infected with *Toxoplasma gondii*, a model of
268 infection-induced pathology (**Figure 5f**). Infected PHD2^{ΔTreg} mice displayed increased
269 weight loss (**Figure 5g**), reduced colon length (**Figure 5h**) and increased frequency of
270 activated cells characterized by an effector-like phenotype (**Figure 5i**) and IFN-γ
271 secretion capacity (**Figure 5j**). Infected PHD2^{ΔTreg} mice also displayed a decrease in
272 Treg T-bet⁺ frequency, a population known to control Th1 inflammation during
273 toxoplasmosis⁵¹ (**Figure 5k**). Overall, PHD2^{ΔTreg} mice displayed an uncontrolled
274 expansion of Th1-like cells following experimental toxoplasmosis. In contrast, both
275 PHD2-deficient and sufficient mouse strains were equally sensitive to enteritis induced
276 upon injection of anti-CD3 antibodies (**Figure 5-figure supplement 1**), a model known
277 to induce the predominant expansion of Th17-like, inflammatory effectors in vivo⁵². The
278 role of uncontrolled IFN-γ secretion in mediating the pro-inflammatory status of this
279 mouse strain was further confirmed by the observation that ubiquitous loss of *Ifng* gene
280 expression largely reversed the phenotypical and cellular altered status of PHD2^{ΔTreg}
281 mice (**Figure 5-figure supplement 2**).

282

283 **Concomitant loss of HIF2 α , but not HIF1 α , expression partially corrects the pro-**
284 **inflammatory phenotype of PHD2 Δ^{Treg} mice.**

285 Based on the notion that HIF1 α and HIF2 α represent well-described targets of PHD2,
286 we established a series of conditional KO mouse strains to identify the molecular
287 pathway responsible for the decreased functional activity of PHD2-deficient Tregs at
288 steady state (**Figure 6**) (see **Figure 6-figure supplement 1** for strain validation). Treg-
289 selective deletion of HIF1 α and HIF2 α expression alone did not significantly alter colon
290 length (used as a proxy for spontaneous inflammation) nor general T cell immune
291 homeostasis (**Figure 6-figure supplement 1**). The same observation was made for
292 double HIF1 α and HIF2 α KOs (data not shown). In marked contrast, combined deletion
293 of PHD2 and HIF2 α reversed some of the inflammatory symptoms observed in
294 PHD2 Δ^{Treg} mice, such as splenomegaly, colon length (**Figure 6a, b**) and hematocrit
295 counts (**Figure 1-figure supplement 2**). Treg specific, PHD2-HIF1 α double KOs were
296 virtually indistinguishable from PHD2 Δ^{Treg} according to these morphological criteria.
297 Noteworthy however, Treg-specific PHD2-HIF1 α double KOs mice were born at sub-
298 mendelian ratios, and displayed a marked weight loss during adult life and reduced
299 viability, indicative of a more pronounced pro-inflammatory status (data not shown). This
300 mouse strain also displayed a tendency toward increased expansion of Th1-like cells in
301 peripheral lymph nodes (**Figure 6e**). PHD2-HIF1 α -HIF2 α triple KOs and PHD2-HIF2 α
302 double KOs displayed a similar phenotype, establishing a predominant role for HIF2 α
303 over HIF1 α in mediating the effects of PHD2 on the capacity of Treg to regulate immune
304 homeostasis at rest. Similarly, lack of HIF2 α expression largely reversed the altered
305 phenotype of conventional T cells induced by loss of Treg-associated PHD2 expression.
306 Indeed, cells from double (PHD2-HIF2 α) and triple (PHD2-HIF1 α -HIF2 α) Treg specific
307 KOs displayed a near normal phenotype (based on CD62L and CD44 expression) and
308 propensity to secrete IFN- γ (**Figure 6c-e**). Finally, loss of Treg-associated expression of
309 HIF2 α also reversed the expansion of Treg numbers (**Figure 6f**) and restored Foxp3
310 protein expression to near-control levels (**Figure 6g**).

311
312 **Transcriptomic analysis identifies cell survival, response to chemokines and**
313 **STAT1-mediated signaling as target pathways of the PHD2-HIF2 α axis in Tregs.**

314 Collectively, the previous observations suggest that the PHD2-HIF2 α regulatory axis
315 confers to Tregs the capacity to control the spontaneous, type-1 like, activity of
316 conventional T cells. To identify PHD2-dependent signaling pathways operating in
317 Tregs, splenic Foxp3-expressing cells were purified from all mouse strains described in
318 this manuscript and their transcriptome analyzed following bulk RNA-seq. A set of 532
319 genes were found differentially expressed between WT and PHD2-deficient Tregs
320 (**Figure 7**) (a summary-list of upregulated and downregulated pathways in PHD2 Δ^{Treg}
321 mice vs Foxp3^{cre} mice is provided in **Figure 7-figure supplement 1**). Differential gene

322 expression analysis between all mouse strains studied identified 1868 genes
323 differentially expressed between groups. An unsupervised clustering of the differentially
324 expressed genes led to the identification of 20 clusters, as shown in **Figure 7a**. To
325 identify gene clusters that were specifically involved in the immune homeostatic control
326 of naive mice, the RNA-seq data were filtered and grouped by k-mean clustering. We
327 next searched for sets of genes whose expression best correlated with an arbitrary
328 inflammatory index, established based on previously described findings (mostly colon
329 length, splenomegaly and spontaneous conventional T cell activation status) and
330 summarized in **Figure 7b**. In particular, while concomitant deletion of HIF1 α expression
331 worsened the inflammatory status of PHD2 Δ Treg mice, loss of HIF2 α expression mitigated
332 most inflammatory-related parameters at rest. We therefore clustered genes according
333 to a “gradient of disease severity” and grouped them in sets of gene whose expression
334 decreased (cluster 10, **Figure 7c**) or increased (cluster 11, **Figure 7d**) accordingly.
335 Gene ontology analysis of these clustered gene sets revealed the following. Reduced
336 expression of cell death-related and gain of survival-associated gene expression
337 correlated with the increased frequency of Tregs in the corresponding mouse strains
338 (**Figure 7c, d**). Not surprisingly, the expression of genes associated with anti-
339 inflammatory responses was gradually lost according to the same severity gradient.
340 Finally, genes, associated with T cell migration, including several chemokine receptors,
341 also displayed an ordered loss of expression along the same gradient (**Figure 7c**). For
342 comparison purposes, genes whose expression was restored to control levels upon
343 combined deletion of PHD2 and HIF1 α were also examined. As expected from
344 previously published findings, these HIF1 α -dependent biological pathways included
345 glycolysis and angiogenesis (**Figure 7e**).

346 Ingenuity Pathway Analysis (IPA) was performed in order to identify possible
347 upstream regulators affecting expression of downstream genes identified in clusters 10
348 and 11. This analysis led to the identification of STAT1 as a putative upstream
349 transcription factor regulating the expression of a set of genes whose expression was
350 altered in PHD2-deficient Tregs (**Figure 8a**). Since *Stat1* mRNA expression was not
351 altered by PHD2 invalidation (as revealed by RNA-Seq analysis), we tested the capacity
352 of STAT1 to undergo phosphorylation in response to IFN- γ . This set of experiments led
353 to the identification of a defective, accumulation of phospho-STAT1 in PHD2-deficient
354 Tregs (**Figure 8b, c**), while the levels of total STAT1 protein appeared unaffected
355 (**Figure 8d**). Noteworthy, concomitant deletion of HIF2 α restored a near control
356 response to IFN- γ in PHD2 deficient Tregs (**Figure 8b-d**). In keeping with the observed
357 pro-inflammatory phenotype associated with these mouse strains, conventional T cells
358 from PHD2 Δ Treg mice displayed an augmented response to IFN- γ (as judged by pSTAT1
359 accumulation), partially reversed in mice bearing Tregs lacking both PHD2 and HIF2 α
360 expression (**Figure 8b, left panel**). Finally, the proportion of Tregs expressing CXCR3,
361 a well described STAT1-dependent chemokine receptor⁵³ was reduced in a HIF2 α -

362 dependent manner in PHD2-deficient Tregs (**Figure 8e**), further strengthening the
363 conclusion that PHD2 expression controls the response of Tregs to IFN- γ .

364

365 **Discussion**

366

367 The present study highlights the important role of the prolyl-hydroxylase PHD2 in the
368 regulation of Treg development and function. Deletion of PHD2 in developing, Tregs led
369 to the accumulation of the subset of Treg precursor characterized by low expression of
370 Foxp3, at the expenses of the mature, Foxp3⁺CD25⁺ Treg population (**Figure 2c**).
371 PHD2-deficient Tregs were nevertheless found in increased numbers in vivo at steady
372 state (**Figure 2a**), albeit with an altered phenotype. In particular, the expression of
373 molecules known to be associated with optimal suppressive activity (such as Foxp3,
374 ICOS and CD25)^{1,54,55} was marginally decreased, while expression of PD-1, a marker
375 associated with altered functional activity of many immune cells including Tregs^{56,57} was
376 augmented. Of note, other molecules known to play an important role in Treg function
377 were expressed at optimal levels (cf CTLA4 and IL-10).

378 Although we have not specifically addressed the role of PHD2 in thymic vs
379 peripherally induced Tregs, it is noteworthy that lack of PHD2 expression altered Treg
380 thymic development, without any major effect on the generation of iTreg in vitro,
381 suggesting a more pronounced role of PHD2 on thymic vs peripherally generated Tregs,
382 although this conclusion should be strengthened by additional studies.

383 Mice selectively lacking PHD2-expression in Treg displayed a proinflammatory
384 phenotype (with early manifestations of gastrointestinal tract inflammation), associated
385 to an elevated hematocrit, enhanced vascular permeability and an altered homeostatic
386 profile of splenic conventional T cells. In marked contrast to WT Tregs, PHD2-deficient
387 Tregs express relatively high levels of *Vegfa* transcripts (as established from RNAseq
388 analysis), a factor known to both increase vascular permeability⁵⁸, and induce
389 erythropoietin (Epo) production from perivascular stromal cells in several organs⁵⁹.
390 Alternatively, since expression of the YFP-Cre allele was found in a minor, proportion of
391 CD45-negative cells in all organs examined (see **Figure 8-figure supplement 1**).
392 PHD2-deletion could result in elevated expression of Epo from a non-hematopoietic
393 source. In any event, analysis of several organs (including spleen, liver and kidney) from
394 PHD2 Δ^{Treg} mice failed to reveal any increase in *Epo* mRNA accumulation (our own
395 unpublished observations), and further studies will therefore be required to identify the
396 mechanism underlying the observed hematological alterations in PHD2 Δ^{Treg} mice.
397 Several observations however strongly indicate that the major, proinflammatory
398 phenotype observed in these mice were due to the specific impairment in Treg function
399 consequent to the loss of PHD2 activity. Despite previous reports describing the
400 stochastic activity of the *Foxp3-Cre-YFP* allele in non-Tregs leading to the recombination

401 of some, but not all alleles⁶⁰, we consistently found a control-level expression of PHD2 in
402 all conventional T cell subset tested (**Figure 1-figure supplement 1**). Secondly, co-
403 transfer of highly purified Tregs with WT naive CD4⁺ conventional target cells clearly
404 demonstrated an intrinsic role of PHD2 in regulating Treg function. Finally, and this will
405 be discussed further below, mice bearing double PHD2-HIF2 α -deficient Tregs recover a
406 near-control phenotype, further excluding a major influence of the genetic background
407 on the observed phenotype. Our observations confirm and further extends observations
408 from a study published during completion of our work⁴⁹, indicating a specific, non-
409 redundant role for PHD2 in controlling Treg activity in vivo.

410 Based on the notion that hypoxia-induced factors represent major substrates of
411 PHD2, we generated a series of mouse strains to evaluate the relative role of HIF1 α and
412 HIF2 α in regulating Treg phenotype and function. The combined loss of PHD2 and
413 HIF2 α but not HIF1 α , corrected some, but not all abnormalities found in the PHD2 Δ^{Treg}
414 mouse strain. To uncover the mechanism whereby the PHD2-HIF2 α axis regulates the
415 capacity of Tregs to exert a homeostatic control over conventional T cells, a large
416 transcriptomic analysis was undertaken. To be able to isolate genes specifically involved
417 in the control of Treg activity in naive animals, we took advantage of the graded pro-
418 inflammatory status of the mouse strain generated (based on colon length and
419 spontaneous activation of Tconv cells, see **Figure 6**) to identify gene clusters whose
420 expression correlated with Treg-mediated immune homeostasis. This analysis led us to
421 identify important pathways providing mechanistic insights into the role of the PHD2-
422 HIF2 α axis in Treg biology. In particular, loss of PHD2 led to an altered expression of
423 genes coding for chemokine receptors and adhesion molecules, suggesting a potential
424 role of this oxygen sensor in chemotaxis and traffic. This conclusion is of particular
425 interest in light of two observations described in this study. As previously discussed,
426 PHD2 Δ^{Treg} mice displayed a selective expansion of Th1-prone effectors in all lymphoid
427 organs examined (**Figure 1**). Accordingly, ubiquitous loss of IFN- γ expression strongly
428 attenuated the pro-inflammatory phenotype of mice with PHD2-deficient Tregs (**Figure**
429 **5-figure supplement 2**), thus suggesting a specific role for PHD2 in endowing Tregs to
430 control Th1-like immune responses in vivo. Secondly, the IPA analysis conducted on the
431 transcriptomic data led to the identification of STAT1 as a potential common regulator of
432 many genes whose expression was under the control of the PHD2-HIF2 α axis, including
433 in particular CXCR3^{53,61}. Based on well-described role for Treg-expressed CXCR3 in
434 modulating Th1-like responses in vivo^{62,63}, and the reduced expression of this
435 chemokine receptor described in the present study (**Figure 8e**), it is tempting to
436 speculate that the reduced capacity of PHD2-deficient Tregs to control Th1 responses is
437 a consequence of an altered STAT1-signaling pathway, leading to reduced CXCR3
438 expression. It is noteworthy that response to CXCR3 ligands has been recently shown to
439 determine the precise positioning of effector and memory CD8 cells in peripheral lymph
440 nodes⁶⁴. Further studies would be required to identify the precise mechanism at work,

441 since the expression of many potential chemokine receptors (including CXCR4, known
442 to exert inhibitory function over other chemokine receptors⁶⁵) and adhesion molecules
443 (such as Ly6a or CD44) appears under the control of the PHD2-HIF2 α axis in Tregs.
444 Whether altered positioning of Tregs within lymphoid organs represents an important
445 factor contributing to the proinflammatory phenotype of PHD2 Δ Treg mice remains
446 however to be thoroughly examined. Similarly, the potential mechanistic link between
447 HIF2 α and STAT1 activation remains to be firmly established by further investigations.

448 Collectively, the observations reported in this study demonstrate a non-redundant
449 role for PHD2 in controlling survival, phenotype, migration properties and the capacity of
450 Tregs to control Th1-like responses. These biological responses appear under the
451 control of HIF2 α , and largely independent of HIF1 α -regulated metabolic pathways.
452 Although the role of the PHD2-HIF2 α axis has been previously highlighted by Yamamoto
453 and colleagues using an alternative, shRNA-based approach⁴⁹, our observations do not
454 fully concur with the previous study on two grounds. First, in contrast to PHD2 knock-
455 down (PHD2-KD) cells, PHD2-genetically deficient Tregs retained full suppressive
456 capacities in vitro. Secondly, no sign of reversal to an effector state were found in PHD2-
457 KO regulatory T cells, whereas downregulation of PHD2 expression led to an increased
458 expression of T-bet, GATA-3 and TNF α . Notably, PHD2-KD Tregs were able to induce
459 skin-graft rejection in the absence of bona-fide effector cells, suggesting a possible
460 acquisition of effector function by these cells. Although these observations are
461 compatible with a possible gene-dosage effect of PHD2 on Treg biology, further studies
462 are needed to identify the mechanism at work in these two experimental models.

463
464 In any events, both studies concur in identifying a possible deleterious role of HIF2 α
465 overactivation in the control of regulatory T cell function. These findings appear at odds
466 with a recent publication by Tzu-Sheng Hsu and colleagues in which deletion of HIF2 α ,
467 but not HIF1 α , expression was found to negatively affect Treg function⁴⁸. Of note,
468 concomitant deletion of both HIF1 α and HIF2 α restored the suppressive activity of
469 Tregs⁴⁸. An elegant hypothesis, put forward by these authors, may help reconcile some
470 of these apparently contradictory observations. Most experimental evidence concurs
471 with a dual role of HIF1 α in Treg differentiation and stability. In setting of sub-optimal
472 Treg-inducing conditions, HIF1 α may promote adequate expression of Foxp3 by
473 differentiating Tregs. Once the Treg phenotype has been fully acquired, HIF1 α protein
474 expression is reduced following interaction with Foxp3⁴⁷, thus explaining the relative lack
475 of influence of HIF1 α on differentiated Tregs. As a consequence, HIF1 α -KO Tregs retain
476 full suppressive activity⁴⁸. The interaction between HIF1 α and Foxp3 can however also
477 lead to Foxp3 protein degradation, and thus Treg instability. Therefore, forced
478 stabilization of HIF1 α (such as observed in triple PHD KOs⁴⁴ or pVHL-deficient Tregs⁶⁶)
479 leads to loss of Foxp3 expression and Treg identity and acquisition of pro-inflammatory
480 functions. Inflammation observed in these mouse strains can be largely attributed to the

481 pro-inflammatory influence of ex-Tregs. As discussed for HIF1 α , HIF2 α also appears to
482 regulate Treg stability, albeit in a different direction. Despite a normal phenotype at rest,
483 mice displaying HIF2 α -deficient Tregs were largely defective in suppressing
484 inflammation in the gut and in the lungs⁴⁸. This pro-inflammatory phenotype was largely
485 explained by the HIF1 α -dependent reprogramming of HIF2 α -deficient Tregs into IL-17
486 secreting cells. Collectively, the available literature points to a central role for HIF1 α in
487 determining Treg stability and function in vivo. Depending on the biological pathway
488 leading to its increased expression and/or protein stabilization, HIF1 α promotes the
489 differentiation of Tregs into IFN- γ (in triple PHD KOs or pVHL-deficient Tregs) or IL-17
490 (in HIF2 α -deficient Tregs) secreting cells. Although the mechanism underlying the
491 acquisition of Th1 vs Th17-like profiles in these models remains to be established, the
492 induction of a glycolytic metabolism is probably instrumental in mediating Treg
493 instability⁶⁷.

494
495 In the present study, loss of HIF1 α expression did not revert the phenotype of PHD2-
496 HIF2 α -deficient Tregs, despite reestablishing a control-like expression of pro-glycolytic
497 genes (**Figure 7e**). Accordingly, PHD2-deficient Tregs did not acquire the capacity to
498 produce pro-inflammatory cytokines (**Figure 1-figure supplement 1**), nor displayed any
499 significant loss of Foxp3 expression upon in vitro culture (**Figure 2k, l**) or in vivo transfer
500 (**Figure 4e**). Thus, the available evidence suggests that in PHD2-sufficient cells, HIF2 α
501 allows adequate Treg function by negating the influence of HIF1 α on Foxp3-expression,
502 while overactivation of HIF2 α activity secondary to the loss of PHD2 expression leads to
503 altered Treg phenotype, most probably via a STAT1-dependent pathway.

504
505 Considering the specific role of PHD2, it is worth mentioning that both the
506 transcriptomic data and our own unpublished observations (indicating an increased
507 sensitivity of triple PHD2-HIF1 α -HIF2 α Tregs specific KO mice to chemical induced
508 colitis) suggest that while the capacity of Tregs to control tissue homeostasis in the
509 naive state is under the predominant control of the PHD2-HIF2 α axis, other, non-HIFs
510 PHD2-substrates³⁰⁻³⁷ probably play an important role in Treg biology under strong
511 inflammatory settings. Finally, the present study suggests that some caution should be
512 exerted in the administration of PHD inhibitors presently considered for the treatment of
513 renal anemia⁶⁸, inflammatory bowel diseases⁶⁹ as well as Parkinson's disease⁷⁰, as
514 these compounds may display some pro-inflammatory effects via the alteration of Treg
515 phenotype and function in vivo.

516

517

Key Resources Table				
Reagent type (species) or resource	Designation	Source or reference	Identifiers	Additional information
Genetic reagent (<i>M. musculus</i>)	C57BL/6	Envigo	RRID:MGI:5658455	Horst, The Netherlands
Genetic reagent (<i>M. musculus</i>)	<i>Egln1^{fl/fl}</i>	The Jackson Laboratory	RRID:IMSR_NM-CKO-2100497	P. Carmeliet (VIB-KULeuven)
Genetic reagent (<i>M. musculus</i>)	<i>Foxp3-Cre-YFP</i>	PMID: 18387831	RRID:IMSR_JA X:016959	A. Liston (KULeuven)
Genetic reagent (<i>M. musculus</i>)	<i>Hif1a^{fl/fl}</i> (Hif1atm3Rsjo/J)	The Jackson Laboratory	RRID:IMSR_JA X:007561	F. Bureau (Liege University)
Genetic reagent (<i>M. musculus</i>)	<i>Epas^{fl/fl}</i> (Epas1tm1Mcs/J)	The Jackson Laboratory	RRID:IMSR_JA X:008407	J.A. Lopez (Madrid University)
Genetic reagent (<i>M. musculus</i>)	<i>lfng^{-/-}</i>	The Jackson Laboratory	RRID:IMSR_CA RD:178	Bar Harbor, ME, USA
Genetic reagent (<i>M. musculus</i>)	CD45.1 (B6.SJL-Ptprca Pepcb/BoyJ)	The Jackson Laboratory	RRID:IMSR_JA X:002014	Bar Harbor, ME, USA
Genetic reagent (<i>M. musculus</i>)	<i>Rag2^{-/-}</i>	The Jackson Laboratory	RRID:IMSR_JA X:008449	Bar Harbor, ME, USA
Antibody	anti-mouse CD278 (Icos)-biotin (C398.4A, mouse monoclonal)	eBioscience	13-9949-82	(1:100)
Antibody	anti-mouse CD27-PeCy7 (LG.7F9, mouse monoclonal)	eBioscience	25-0271-82	(1:250)
Antibody	anti-mouse Foxp3-FITC (FJK-16s, mouse monoclonal)	eBioscience	71-5775-40	(1:100)
Antibody	anti-mouse ROR γ t-PE (B2D, mouse monoclonal)	eBioscience	12-6981-82	(1:100)
Antibody	anti-mouse T-bet-PE (4B10,	eBioscience	12-5825-82	(1:100)

	mouse monoclonal)			
Antibody	anti-mouse PD1-PECF594 (J43, mouse monoclonal)	BD Biosciences	562523 RRID : AB_2737634	(1:100)
Antibody	anti-mouse CXCR3-APC (CXCR3-173, mouse monoclonal)	BD Biosciences	562266 RRID : AB_11153500	(3:500)
Antibody	anti-mouse CD24-PECF594 (M1/69, mouse monoclonal)	BD Biosciences	562477 RRID : AB_11151917	(1:100)
Antibody	anti-mouse CD25-BB515 (PC61, mouse monoclonal)	BD Biosciences	564424 RRID : AB_2738803	(1:100)
Antibody	anti-mouse CD44-PECy7 (IM7, mouse monoclonal)	BD Biosciences	560569 RRID : AB_1727484	(1:100)
Antibody	anti-mouse CD4-A700 (RM4-5, mouse monoclonal)	BD Biosciences	557956 RRID : AB_396956	(3:500)
Antibody	anti-mouse CD8-A700 (53-6.7, mouse monoclonal)	BD Biosciences	557959 RRID : AB_396959	(3:500)
Antibody	anti-mouse CD4-PB (RM4-5, mouse monoclonal)	BD Biosciences	558107 RRID : AB_397030	(1:100)
Antibody	anti-mouse CD62L-A700 (MEL-14, mouse monoclonal)	BD Biosciences	560517 RRID : AB_1645210	(1:100)
Antibody	anti-mouse GATA3-PE (L50-823, mouse monoclonal)	BD Biosciences	560074 RRID : AB_1645330	(1:10)
Antibody	anti-mouse RORyt-PECF594	BD Biosciences	562684 RRID : AB_2651150	(1:200)

	(Q31-378, mouse monoclonal)			
Antibody	anti-mouse STAT1 (pY701)-A488(4a, mouse monoclonal)	BD Biosciences	612596 RRID : AB_399879	(1:10)
Antibody	anti-mouse IFN γ -PE (XMG1.2, mouse monoclonal)	BD Biosciences	554412 RRID : AB_395376	(1:100)
Antibody	anti-mouse IL-10-APC (JES5-16E3, mouse monoclonal)	BD Biosciences	554468 RRID : AB_398558	(1:100)
Antibody	anti-mouse IL-17-PerCP-Cy5.5 (N49-653, mouse monoclonal)	BD Biosciences	560799 RRID : AB_2033981	(1:100)
Antibody	anti-CD3 antibody (2c11, mouse monoclonal)	BioXcell	145-2c11	20 μ g/mouse
peptide, recombinant protein	streptavidin-PECy7.	BD Biosciences	RRID :557598 AB_10049577	(1:100)
peptide, recombinant protein	IFN- γ protein	Peprotech	315-05	50 ng/mL
Chemical compound, drug	Evans blue	Sigma	314-13-6	0.5%
Chemical compound, drug	Brefeldin-A	eBioscience	00-4506-51	(1:1000)
Chemical compound, drug	Dextran Sodium Sulfate, colitis grade (36,000 - 50,000 Da)	MP Biomedical	160110	2%
Commercial assay or kit	LIVE/DEAD kit	Invitrogen	L10119	(1:1000)
Commercial assay or kit	anti-CD90.2 beads MACS	Miltenyi	130-121-278	(1:5)
Commercial assay or kit	anti-CD4 beads MACS	Miltenyi	130-117-043	(1:3)

Sequence-based reagent	<i>Egln1 (PHD2)_F</i>	This paper	PCR primers	AGGCTATGTCC GTCACGTTG
Sequence-based reagent	<i>Egln1 (PHD2)_R</i>	This paper	PCR primers	TACCTCCACTT ACCTTGGCG
Sequence-based reagent	<i>Egln2 (PHD1)_F</i>	This paper	PCR primers	TCACGTGGACG CAGTAATCC
Sequence-based reagent	<i>Egln2 (PHD1)_R</i>	This paper	PCR primers	CGCCATGCACC TTAACATCC
Sequence-based reagent	<i>Egln3 (PHD3)_F</i>	This paper	PCR primers	AGGCAATGGTG GCTTGCTAT
Sequence-based reagent	<i>Egln3 (PHD3)_R</i>	This paper	PCR primers	GACCCCTCCGT GTAACCTGG
Sequence-based reagent	<i>Hif1a_F</i>	This paper	PCR primers	CATCAGTTGCC ACTTCCCA
Sequence-based reagent	<i>Hif1a_R</i>	This paper	PCR primers	GGCATCCAGAA GTTTTCTCACA C
Sequence-based reagent	<i>Epas1 (HIF2a)_F</i>	This paper	PCR primers	ACGGAGGTCTT CTATGAGTTGG C
Sequence-based reagent	<i>Epas1 (HIF2a)_R</i>	This paper	PCR primers	GTTATCCATTTG CTGGTCGGC
Sequence-based reagent	<i>lfng_F</i>	This paper	PCR primers	TGCCAAGTTTG AGGTCAACA
Sequence-based reagent	<i>lfng_R</i>	This paper	PCR primers	GAATCAGCAGC GACTCCTTT
Sequence-based reagent	<i>Il12a_F</i>	This paper	PCR primers	CCTCAGTTTGG CCAGGGTC
Sequence-based reagent	<i>Il12a_R</i>	This paper	PCR primers	CAGGTTTCGGG ACTGGCTAAG
Sequence-based reagent	<i>Il10_F</i>	This paper	PCR primers	CCTGGGTGAGA AGCTGAAGA
Sequence-based reagent	<i>Il10_R</i>	This paper	PCR primers	GCTCCACTGCC TTGCTCTTA
Sequence-based reagent	<i>Il17a_F</i>	This paper	PCR primers	ATCCCTCAAAG CTCAGCGTGTC
Sequence-based reagent	<i>Il17a_R</i>	This paper	PCR primers	GGGTCTTCATT GCGGTGGAGA G
Sequence-based reagent	<i>Il1b_F</i>	This paper	PCR primers	CAAGCTTCCTT GTGCAAGTG
Sequence-based reagent	<i>Il1b_R</i>	This paper	PCR primers	AGGTGGCATTT CACAGTTGA
Sequence-based reagent	<i>Il4_F</i>	This paper	PCR primers	ATGCACGGAGA TGGATGTG
Sequence-based reagent	<i>Il4_R</i>	This paper	PCR primers	AATATGCGAAG CACCTTGGA
Sequence-based reagent	<i>Il6_F</i>	This paper	PCR primers	GTTCTCTGGGA AATCGTGGA

Sequence-based reagent	<i>Ii6_R</i>	This paper	PCR primers	GCAAGTGCATC ATCGTTGTT
Sequence-based reagent	<i>Rpl32_F</i>	This paper	PCR primers	ACATCGGTTAT GGGAGCAAC
Sequence-based reagent	<i>Rpl32_R</i>	This paper	PCR primers	TCCAGCTCCTT GACATTGT
Sequence-based reagent	<i>Tnfa_F</i>	This paper	PCR primers	GCCTCCCTCTC ATCAGTTCTA
Sequence-based reagent	<i>Tnfa_R</i>	This paper	PCR primers	GCTACGACGTG GGCTACAG
Sequence-based reagent	<i>Ii12b_F</i>	This paper	PCR primers	ATGTGTCCTCA GAAGCTAACC
Sequence-based reagent	<i>Ii12b_R</i>	This paper	PCR primers	CTAGGATCGGA CCCTGCAGGGA AC
Software, algorithm	Prism 6	GraphPad	RRID:SCR_002 798	Version 6.0

519
520 **Mice.** C57BL/6 mice were purchased from Envigo (Horst, The Netherlands). *Egln1^{fl/fl}*
521 mice were provided by P. Carmeliet (VIB-KULeuven, Leuven, Belgium); *Foxp3-Cre-YFP*
522 mice, developed by A. Rudensky⁷¹ were kindly provided by A. Liston (KULeuven,
523 Leuven, Belgium); *Hif1atm3Rsjo/J (Hif1a^{fl/fl})* mice were kindly provided by F. Bureau
524 (Liege University, Liege, Belgium); *Epas1tm1Mcs/J (Epas^{fl/fl})* mice were provided by J.A.
525 Lopez (Madrid University, Madrid, Spain); *Ifng^{-/-}*, CD45.1 (B6.SJL-Ptprc^a Pepc^b/Boy^J)
526 and *Rag2^{-/-}* mice were obtained from The Jackson Laboratory (Bar Harbor, ME, USA).
527 All mice were backcrossed for more than 10 generations into a C57BL/6 background
528 and housed in individually ventilated cages. *Foxp3-Cre-YFP* mice were crossed with
529 *Egln1^{fl/fl}*, *Hif1a^{fl/fl}*, *Epas^{fl/fl}* to produce mice with Treg-specific deletion of PHD2, HIF1α,
530 HIF2α, PHD2-HIF1α, PHD2-HIF2α or PHD2-HIF1α-HIF2α. Heterozygous *Foxp3^{cre/+}*
531 *Egln1^{fl/fl}* mice were generated by crossing the *Foxp3-Cre-YFP* mice with *Egln1^{fl/fl}* mice. All
532 mice were used between 8 and 14 weeks of age. PHD2-sufficient mice (expressing
533 *Foxp3-Cre-YFP*, or floxed forms of PHD2, HIF1α and HIF2α-encoding alleles and
534 generated as littermates in our colony) were used as appropriate controls in the early
535 stages of this work. These mice displayed a phenotype indistinguishable from WT mice
536 and were therefore considered as a single experimental group throughout this study in
537 order to reach statistical significance in all experiments. The experiments were carried
538 out in compliance with the relevant laws and institutional guidelines and were approved
539 by the Université Libre de Bruxelles Institutional Animal Care and Use Committee
540 (protocol number CEBEA-4).
541

542 **Antibodies, intracellular staining and flow cytometry.** The following monoclonal
543 antibodies were purchased from eBioscience: CD278 (ICOS)-biotin, CD27-PeCy7,
544 *Foxp3-FITC*, RORγt-PE, T-bet-PE; or from BD Biosciences: PD1-PECF594, CXCR3-
545 APC, CD24-PECF594, CD25-BB515, CD44-PECy7, CD4-A700, CD8-A700, CD4-PB,

546 CD62L-A700, GATA3-PE, ROR γ t-PECF594, STAT1 (pY701)-A488, IFN γ -PE, IL-10-
547 APC, IL-17-PerCP-Cy5.5, streptavidin-PECy7. Live/dead fixable near-IR stain
548 (ThermoFisher) was used to exclude dead cells. For transcription factor staining, cells
549 were stained for surface markers, followed by fixation and permeabilization before
550 nuclear factor staining according to the manufacturer's protocol (Foxp3 staining buffer
551 set from eBioscience). For cytokine staining, cells were stimulated in media containing
552 phorbol 12-myristate 13-acetate (50ng/mL, Sigma-Aldrich), ionomycin (250ng/mL,
553 Sigma-Aldrich) and brefeldin-A (1/100, eBioscience) for 3h. After stimulation, cells were
554 stained for surface markers, followed by fixation and permeabilization before intracellular
555 staining according to the manufacturer's protocol (cytokine staining buffer set from BD
556 Biosciences). For phosphorylation staining, cells were stimulated with IFN- γ (50 ng/mL,
557 Peprotech) for 30 min, fixed with formaldehyde and permeabilized with methanol before
558 staining. Flow cytometric analysis was performed on a Canto II (BD Biosciences) and
559 analyzed using FlowJo software (Tree Star).

560 **T cell cultures.** After removal of Peyer's patches and mesenteric fat, intestinal tissues
561 were washed in HBSS 3% FCS and PBS, cut in small sections and incubated in HBSS
562 3% FCS containing 2,5mM EDTA and 72,5 μ g/mL DTT for 30 min at 37°C with agitation
563 to remove epithelial cells, and then minced and dissociated in RPMI containing liberase
564 (20 μ g/ml, Roche) and DNase (400 μ g/ml, Roche) at 37 °C for 30 min. Leukocytes were
565 collected after a 30% Percoll gradient (GE Healthcare). Lymph nodes and spleens were
566 mechanically disrupted in culture medium. CD4⁺ T cells were positively selected from
567 organ cell suspensions by magnetic-activated cell sorting using CD4 beads (MACS,
568 Miltenyi) according to the manufacturer's protocol, and purified as CD4⁺
569 CD44^{lo}CD62L^{hi}CD25⁻ or CD4⁺ CD44^{lo} CD62L^{hi} YFP⁻ by fluorescence activated cell
570 sorting. T cells were cultured at 37°C in RPMI supplemented with 5% heat-inactivated
571 FBS (Sigma-Aldrich), 1% non-essential amino acids (Invitrogen), 1 mM sodium pyruvate
572 (Invitrogen), 2 mM L-glutamin (Invitrogen), 500 U/mL penicillin/500 μ g/ml streptomycin
573 (Invitrogen), and 50 μ M β -mercaptoethanol (Sigma-Aldrich). To generate iTreg cells,
574 cells were cultured in 24 well plates coated with 5 μ g/mL anti-CD3 (BioXcell, clone 145-
575 2C11) at 37°C for 72h. The culture was supplemented with anti-CD28 (1 μ g/mL,
576 BioXcell, clone 37.51), TGF- β (3 ng/ml, eBioscience) and IL-2 (10 ng/mL, Peprotech) for
577 optimal iTreg cell polarization.
578

579 **Treg cell suppression assays.** *In vitro* assay. CD4⁺ CD44^{lo}CD62L^{hi} CD25⁻ naive T
580 cells were isolated from the spleen of CD45.1⁺ mice by cell sorting after positive
581 enrichment for CD4⁺ cells using MACS LS columns (Miltenyi) and labelled with
582 carboxyfluorescein diacetate succinimidyl ester (CFSE, ThermoFisher). CD4⁺YFP⁺ Treg
583 cells were isolated from the spleen of Foxp3^{cre} or PHD2 Δ Treg mice by cell sorting.
584 Splenocytes from wild-type B6 mice were depleted in T cells (anti-CD90.2 beads,
585 MACS, Miltenyi) using MACS LS columns (Miltenyi) and used as feeder cells. 4 \times 10⁴
586 CFSE-labelled naive T cells were cultured for 72 h with feeder cells (1 \times 10⁵) and

587 soluble anti-CD3 (0,5 µg/mL) in the presence or absence of various numbers of Treg
588 cells as indicated.

589 *In vivo assay:* *Rag2*^{-/-} mice were injected i.v with a mixture of naive, CFSE labeled, CD4⁺
590 T cells (CD45.1⁺ CD4⁺ CD44^{lo} CD62L^{hi} CD25⁻) (1 x 10⁶) and splenic Treg from *Foxp3*^{cre}
591 or *PHD2*^{ΔTreg} mice (3.3 x 10⁵). Six days after the injection, *Rag2*^{-/-} mice were sacrificed
592 and CD4⁺ T cells proliferation and activation analyzed by flow cytometry.
593

594 **DSS-induced colitis.** *Foxp3*^{cre} or *PHD2*^{ΔTreg} mice were provided with 2% DSS (MP
595 Biomedical, 160110) in tap water for five days. On day 5, the DSS-containing water was
596 replaced with normal drinking water and mice were followed during 14 days for body
597 weight, survival, and colitis severity. Colitis severity score was assessed by examining
598 weight loss, feces consistency and hematochezia (Hemocult SENSA, Mckesson
599 Medical-Surgical, 625078) as described in ref ⁷². Colon samples were washed with PBS
600 and rolled from the distal to proximal end, transected with a needle and secured by
601 bending the end of the needle and fixed in fresh 4% paraformaldehyde (Sigma-Aldrich)
602 overnight and further subjected to routine histological procedures for embedment in
603 paraffin and hematoxylin and eosin (H&E) staining. Tissues were analyzed and scored
604 in a blinded fashion by an independent histopathologist and representative images were
605 subsequently chosen to illustrate key histological findings.
606

607 **Toxoplasma infection.** ME-49 type II *Toxoplasma gondii* was kindly provided by Dr De
608 Craeye (Scientific Institute of Public Health, Belgium) and was used for the production of
609 tissue cysts in C57BL/6 mice previously (1-3 month) inoculated with three cysts by
610 gavage. Animals were killed, and the brains were removed. Tissue cysts were counted
611 and mice were infected by intragastric gavage with 10 cysts. Mice were sacrificed at day
612 8 after infection.
613

614 **Anti-CD3 mAb-induced enteritis.** Mice were injected i.p. with a CD3-specific antibody
615 (clone 145-2C11, BioXcell 20 µg/mouse) on days 0 and 2 and weighted daily. Mice were
616 sacrificed on day 3 and cytokine production evaluated by qPCR as indicated in the figure
617 legend.
618

619 **Hematological analysis.** Mice blood was obtained from the submandibular vein and
620 collected into heparin prefilled tubes. Blood samples were analyzed using a Sysmex KX-
621 21 N Automated Hematology Analyzer.
622

623 **Evans blue assay.** Blood vessel permeability was assessed as previously described⁷³.
624 Briefly, 200 µL of a 0.5% sterile solution of Evans blue (Sigma) in PBS was i.v injected in
625 mice. After 30 min, organs were collected, weighted and were put in formamide. After 24
626 hours in a 55°C water bath, absorbance was measured at 600 nm.
627

628 **RT-qPCR.** RNA was extracted using the TRIzol method (Invitrogen) and reverse
629 transcribed with Superscript II reverse transcriptase (Invitrogen) according to the
630 manufacturer's instructions. Quantitative real-time RT-PCR was performed using the
631 SYBR Green Master mix kit (ThermoFisher). Primer sequences were as follows:

632 *Rpl32* (F) ACATCGGTTATGGGAGCAAC; *Rpl32* (R) TCCAGCTCCTTGACATTGT; *Il1b*
633 (F) CAAGCTTCCTTGTGCAAGTG; *Il1b* (R) AGGTGGCATTTCACAGTTGA; *Il10* (F)
634 CCTGGGTGAGAAGCTGAAGA; *Il10* (R) GCTCCACTGCCTTGCTCTTA; *Ifng* (F)
635 TGCCAAGTTTGAGGTCAACA; *Ifng* (R) GAATCAGCAGCGACTCCTTT; *Il6* (F)
636 GTTCTCTGGGAAATCGTGGA; *Il6* (R) GCAAGTGCATCATCGTTGTT; *Il17a* (F)
637 ATCCCTCAAAGCTCAGCGTGTC; *Il17a* (R) GGGTCTTCATTGCGGTGGAGAG; *Il12a*
638 (F) CCTCAGTTTGGCCAGGGTC; *Il12a* (R) CAGGTTTCGGGACTGGCTAAG; *Il12b* (F)
639 ATGTGTCCTCAGAAGCTAACC; *Il12b* (R) CTAGGATCGGACCCTGCAGGGAAC; *Tnfa*
640 (F) GCCTCCCTCTCATCAGTTCTA; *Tnfa* (R) GCTACGACGTGGGCTACAG; *Egln1* (F)
641 AGGCTATGTCCGTCACGTTG; *Egln1* (R) TACCTCCACTTACCTTGGCG; *Hif1a* (F)
642 CATCAGTTGCCACTTCCCCA; *Hif1a* (R) GGCATCCAGAAGTTTTCTCACAC; *Epas1*
643 (F) ACGGAGGTCTTCTATGAGTTGGC; *Epas1* (R) GTTATCCATTTGCTGGTCCGC.
644

645 **RNA Sequencing and analysis.** All RNA-Seq analyses were performed using ≥ 2
646 biological replicates. Total RNA was prepared from purified splenic Treg cells using the
647 TRIzol method (Invitrogen). 200 ng of total RNA was subsequently used to prepare
648 RNA-Seq library by using TruSeq RNA sample prep kit (Illumina) according to
649 manufacturer's instructions. Paired-end RNA sequencing was performed on a Novaseq
650 6000 (Illumina) (BRIGHTcore joint facility, ULB-VUB, Brussels, Belgium). Sequenced
651 reads were aligned to the mouse genome (NCBI37/mm9) and uniquely mapped reads
652 were used to calculate gene expression. Data analysis was performed using R program
653 (Deseq2 package). Differentially expressed genes are considered significant when the
654 FDR (false discovery rate or adjusted p-value) < 0.05 and the \log_2FC (fold change) $>$
655 0.5. Upstream regulators analysis was performed following Ingenuity pathway analysis
656 (IPA). IPA predicts functional regulatory networks from gene expression data and
657 provides a significance score (p-value) for each network according to the fit of the
658 network to the set of genes in the database.
659

660 **Statistical analysis.** All statistical analyses were conducted using GraphPad Prism
661 (GraphPad Software). Statistical difference between two groups was determined by an
662 unpaired, two-tailed student's t tests. A one-way or two-way ANOVA was used for
663 multigroup comparisons together with Tukey's multiple comparisons post hoc tests.
664 Survival significance in DSS-induced colitis was determined by a Log-rank Mantel-Cox
665 test. Data is judged to be statistically significant when p value < 0.05 . In figures,
666 asterisks denote statistical significance (*, p < 0.05 ; **, p < 0.01 ; ***, p < 0.001 ; ****, p $<$
667 0.0001).
668

669
670
671
672
673
674
675
676
677
678
679
680
681
682
683
684
685
686
687
688
689
690
691
692
693
694
695
696
697
698
699
700
701
702
703
704
705
706
707
708
709
710
711
712
713
714

References

1. Lu, L., Barbi, J. & Pan, F. The regulation of immune tolerance by FOXP3. *Nat. Rev. Immunol.* **17**, 703–717 (2017).
2. Xing, Y. & Hogquist, K. A. T-Cell Tolerance: Central and Peripheral. *Cold Spring Harb Perspect Biol* **4**, 1–15 (2012).
3. Dominguez-Villar, M. & Hafler, D. A. Regulatory T cells in autoimmune disease. *Nat. Immunol.* **19**, 665–673 (2018).
4. Samstein, R. M., Josefowicz, S. Z., Arvey, A., Treuting, P. M. & Rudensky, A. Y. Extrathymic generation of regulatory T cells in placental mammals mitigates maternal-fetal conflict. *Cell* **150**, 29–38 (2012).
5. Togashi, Y., Shitara, K. & Nishikawa, H. Regulatory T cells in cancer immunosuppression — implications for anticancer therapy. *Nat. Rev. Clin. Oncol.* (2019).
6. Aandahl, E. M., Michaëlsson, J., Moretto, W. J., Hecht, F. M. & Nixon, D. F. Human CD4⁺ CD25⁺ Regulatory T Cells Control T-Cell Responses to Human Immunodeficiency Virus and Cytomegalovirus Antigens. *J. Virol.* **78**, 2454–2459 (2004).
7. Van Der Burg, S. H. *et al.* Association of cervical cancer with the presence of CD4⁺ regulatory T cells specific for human papillomavirus antigens. *PNAS* **104**, 12087–12092 (2007).
8. Caridade, M., Graca, L. & Ribeiro, R. M. Mechanisms underlying CD4⁺ Treg immune regulation in the adult: From experiments to models. *Front. Immunol.* **4**, 1–9 (2013).
9. Clement, R. L. *et al.* Follicular regulatory T cells control humoral and allergic immunity by restraining early B cell responses. *Nat. Immunol.* **20**, 1360–1371 (2019).
10. Vignali, D. A. A., Collison, L. W. & Workman, C. J. How regulatory T cells work. *Nat. Rev. Immunol.* **8**, 523–532 (2008).
11. Wardell, C. M., MacDonald, K. N., Levings, M. K. & Cook, L. Cross talk between human regulatory T cells and antigen-presenting cells: Lessons for clinical applications. *Eur. J. Immunol.* **51**, 27–38 (2021).
12. Shevryev, D. & Tereshchenko, V. Treg Heterogeneity, Function, and Homeostasis. *Front. Immunol.* **10**, 1–13 (2020).
13. Panduro, M., Benoist, C. & Mathis, D. Tissue Tregs. *Annu. Rev. Immunol.* **34**, 609–633 (2016).
14. Ast, T. & Mootha, V. K. Oxygen and mammalian cell culture: are we repeating the experiment of Dr. Ox? *Nat. Metab.* **1**, 858–860 (2019).
15. McKeown, S. R. Defining normoxia, physoxia and hypoxia in tumours - Implications for treatment response. *Br. J. Radiol.* **87**, 1–12 (2014).
16. Bartels, K., Grenz, A. & Eltzschig, H. K. Hypoxia and inflammation are two sides of the same coin. *PNAS* **110**, 18351–18352 (2013).
17. Nanduri, J. *et al.* HIF-1 α activation by intermittent hypoxia requires NADPH oxidase stimulation by xanthine oxidase. *PLoS One* **10**, 1–12 (2015).
18. Mempel, T. R. & Marangoni, F. Guidance factors orchestrating regulatory T cell positioning in tissues during development, homeostasis, and response. *Immunol.*

- 715 *Rev.* **289**, 129–141 (2019).
- 716 19. Hirota, K. Basic biology of hypoxic responses mediated by the transcription factor
717 HIFs and its implication for medicine. *Biomedicines* **8**, (2020).
- 718 20. Baik, A. H. & Jain, I. H. Turning the Oxygen Dial: Balancing the Highs and Lows.
719 *Trends Cell Biol.* **30**, 516–536 (2020).
- 720 21. Wang, G. L. & Semenza, G. L. Purification and characterization of hypoxia-
721 inducible factor. *Journal of Biological Chemistry* **270**, 1230–1237 (1995).
- 722 22. James D Webb, M. L. C. & Pugh, C. W. Hypoxia, hypoxia-inducible factors (HIF),
723 HIF hydroxylases and oxygen sensing. *Cell. Mol. Life Sci.* **66**, 3539–3554 (2009).
- 724 23. Semenza, G. L. HIF-1, O₂, and the 3 PHDs: How animal cells signal hypoxia to
725 the nucleus. *Cell* **107**, 1–3 (2001).
- 726 24. Maxwell, P. H. *et al.* The tumour suppressor protein VHL targets hypoxia-inducible
727 factors for oxygen-dependent proteolysis. *Nature* **44**, 271–275 (1999).
- 728 25. Downes, N. L., Laham-Karam, N., Kaikkonen, M. U. & Ylä-Herttuala, S. Differential
729 but Complementary HIF1 α and HIF2 α Transcriptional Regulation. *Mol. Ther.* **26**,
730 1735–1745 (2018).
- 731 26. Watts, E. R. & Walmsley, S. R. Inflammation and Hypoxia: HIF and PHD Isoform
732 Selectivity. *Trends Mol. Med.* **25**, 33–46 (2019).
- 733 27. Talks, K. L. *et al.* The expression and distribution of the hypoxia-inducible factors
734 HIF-1 α and HIF-2 α in normal human tissues, cancers, and tumor-associated
735 macrophages. *Am. J. Pathol.* **157**, 411–421 (2000).
- 736 28. Hu, C.-J., Sataur, A., Wang, L., Chen, H. & Simon, M. C. The N-Terminal
737 Transactivation Domain Confers Target Gene Specificity of Hypoxia-inducible
738 Factors HIF-1 α and HIF-2 α . *Mol. Biol. Cell* **18**, 986–994 (2007).
- 739 29. Bono, H. & Hirota, K. Meta-analysis of hypoxic transcriptomes from public
740 databases. *Biomedicines* **8**, (2020).
- 741 30. Meneses, A. M. and & Wielockx, B. PHD2 : from hypoxia regulation to disease
742 progression. *Dovepress* 53–67 (2016).
- 743 31. Mikhaylova, O. *et al.* The von Hippel-Lindau Tumor Suppressor Protein and Egl-9-
744 Type Proline Hydroxylases Regulate the Large Subunit of RNA Polymerase II in
745 Response to Oxidative Stress. *Mol. Cell. Biol.* **28**, 2701–2717 (2008).
- 746 32. Denise A. Chan *et al.* Tumor Vasculature is Regulated by PHD2-mediated
747 Angiogenesis and Bone Marrow-Derived Cell Recruitment. *Cancer Cell.* **15**, 527–
748 538 (2009).
- 749 33. Romero-Ruiz, A. *et al.* Prolyl hydroxylase-dependent modulation of eukaryotic
750 elongation factor 2 activity and protein translation under acute hypoxia. *J. Biol.*
751 *Chem.* **287**, 9651–9658 (2012).
- 752 34. Huo, Z. *et al.* Prolyl hydroxylase domain protein 2 regulates the intracellular cyclic
753 AMP level in cardiomyocytes through its interaction with phosphodiesterase 4D.
754 *Biochem. Biophys. Res. Commun.* **427**, 73–79 (2012).
- 755 35. Xie, L. *et al.* PHD2/3-dependent hydroxylation tunes cardiac response to β -
756 adrenergic stress via phospholamban. *J. Clin. Invest.* **125**, 2759–2771 (2015).
- 757 36. Lee, D. C. *et al.* A lactate-induced response to hypoxia. *Cell* **161**, 595–609 (2015).
- 758 37. Guo, J. *et al.* pVHL suppresses kinase activity of Akt in a proline-hydroxylation-
759 dependent manner. *Science* **353**, 929–932 (2016).
- 760 38. Cockman, M. E. *et al.* Lack of activity of recombinant HIF prolyl hydroxylases
761 (PHDs) on reported non-HIF substrates. *Elife* **8**, 1–27 (2019).

- 762 39. Corrado, C. & Fontana, S. Hypoxia and HIF signaling: One axis with divergent
763 effects. *Int. J. Mol. Sci.* **21**, 1–17 (2020).
- 764 40. McGettrick, A. F. & O'Neill, L. A. J. The Role of HIF in Immunity and Inflammation.
765 *Cell Metab.* **32**, 524–536 (2020).
- 766 41. Shi, L. Z. *et al.* HIF1alpha-dependent glycolytic pathway orchestrates a metabolic
767 checkpoint for the differentiation of TH17 and Treg cells. *J. Exp. Med.* **208**, 1367–
768 76 (2011).
- 769 42. Dang, E. V. *et al.* Control of TH17/Treg balance by hypoxia-inducible factor 1. *Cell*
770 **146**, 772–784 (2011).
- 771 43. Shehade, H., Acolty, V., Moser, M. & Oldenhove, G. Cutting Edge: Hypoxia-
772 Inducible Factor 1 Negatively Regulates Th1 Function. *J. Immunol.* **195**, 1372–6
773 (2015).
- 774 44. Clever, D. *et al.* Oxygen Sensing by T Cells Establishes an Immunologically
775 Tolerant Metastatic Niche. *Cell* **166**, 1117-1131.e14 (2016).
- 776 45. Lukashev, D., Caldwell, C., Ohta, A., Chen, P. & Sitkovsky, M. Differential
777 Regulation of Two Alternatively Spliced Isoforms of Hypoxia-inducible Factor-1 α in
778 Activated T Lymphocytes. *J. Biol. Chem.* **276**, 48754–48763 (2001).
- 779 46. Ben-shoshan, J., Maysel-auslender, S., Mor, A., Keren, G. & George, J. Hypoxia
780 controls CD4+ CD25+ regulatory T-cell homeostasis via hypoxia-inducible factor-1
781 a. *Eur. J. Immunol.* 2412–2418 (2008).
- 782 47. Clambey, E. T. *et al.* Hypoxia-inducible factor-1 alpha – dependent induction of
783 FoxP3 drives regulatory T-cell abundance and function during inflammatory
784 hypoxia of the mucosa. *PNAS* **109**, (2012).
- 785 48. Hsu, T. S. *et al.* HIF-2 α is indispensable for regulatory T cell function. *Nat.*
786 *Commun.* **11**, 1–16 (2020).
- 787 49. Yamamoto, A. *et al.* Systemic silencing of Phd2 causes reversible immune
788 regulatory dysfunction. *J. Clin. Invest.* **129**, 3640–3656 (2019).
- 789 50. Owen, D. L. *et al.* Thymic regulatory T cells arise via two distinct developmental
790 programs. *Nat. Immunol.* **20**, 195–205 (2019).
- 791 51. Wohlfert, E. A., Warunek, J., Jin, R. M. & Marzullo, B. Tbet - expressing Tregs
792 protect against lethal immunopathology during T . gondii infection. *J Immunol* **204**,
793 2020 (2020).
- 794 52. Esplugues, E. *et al.* Control of TH17 cells occurs in the Small Intestine. *Nature*
795 **475**, 514–518 (2012).
- 796 53. Hall, A. O. H. *et al.* The Cytokines Interleukin 27 and Interferon- γ Promote Distinct
797 Treg Cell Populations Required to Limit Infection-Induced Pathology. *Immunity* **37**,
798 511–523 (2012).
- 799 54. Fontenot, J. D., Gavin, M. A. & Rudensky, A. Y. Foxp3 programs the development
800 and function of CD4+CD25+ regulatory T cells. *J. Immunol.* **4**, 986–992 (2003).
- 801 55. Redpath, S. A. *et al.* ICOS controls Foxp3+ regulatory T-cell expansion,
802 maintenance and IL-10 production during helminth infection. *Eur. J. Immunol.* **43**,
803 705–715 (2013).
- 804 56. Lowther, D. E. *et al.* PD-1 marks dysfunctional regulatory T cells in malignant
805 gliomas. *JCI* **1**, 1–15 (2016).
- 806 57. Tan, C. L. *et al.* PD-1 restraint of regulatory T cell suppressive activity is critical for
807 immune tolerance. *J. Exp. Med.* **218**, (2021).
- 808 58. Bates, D. O. Vascular endothelial growth factors and vascular permeability.

- 809 *Cardiovasc. Res.* **87**, 262–271 (2010).
- 810 59. Greenwald, A. C. *et al.* VEGF expands erythropoiesis via hypoxia-independent
811 induction of erythropoietin in noncanonical perivascular stromal cells. *J. Exp. Med.*
812 **216**, 215–230 (2019).
- 813 60. Franckaert, D. *et al.* Promiscuous Foxp3-cre activity reveals a differential
814 requirement for CD28 in Foxp3 + and Foxp3-T cells. *Immunol. Cell Biol.* **93**, 417–
815 423 (2015).
- 816 61. Koch, M. A. *et al.* The transcription factor T-bet controls regulatory T cell
817 homeostasis and function during type 1 inflammation. *Nat. Immunol.* **10**, 595–602
818 (2009).
- 819 62. Levine, A. G. *et al.* Stability and function of regulatory T cells expressing the
820 transcription factor T-bet. *Nature* **546**, 421–425 (2017).
- 821 63. Littringer, K. *et al.* Common features of regulatory T cell specialization during Th1
822 responses. *Front. Immunol.* **9**, 1–15 (2018).
- 823 64. Duckworth, B. C. *et al.* Effector and stem-like memory cell fates are imprinted in
824 distinct lymph node niches directed by CXCR3 ligands. *Nat. Immunol.* (2021).
- 825 65. Biasci, D. *et al.* CXCR4 inhibition in human pancreatic and colorectal cancers
826 induces an integrated immune response. *PNAS* **117**, 28960–28970 (2020).
- 827 66. Lee, J. H., Elly, C., Park, Y. & Liu, Y. C. E3-Ubiquitin Ligase VHL Regulates
828 Hypoxia-Inducible Factor-1a to Maintain Regulatory T Cell Stability and
829 Suppressive Capacity. *Immunity* **42**, 1062–1074 (2015).
- 830 67. Shi, H. & Chi, H. Metabolic Control of Treg Cell Stability, Plasticity, and Tissue-
831 Specific Heterogeneity. *Front. Immunol.* **10**, 1–17 (2019).
- 832 68. Gupta, N. & Wish, J. B. Hypoxia-Inducible Factor Prolyl Hydroxylase Inhibitors:
833 Potential New Treatment for Anemia in Patients With CKD. *Am. J. Kidney Dis.* **69**,
834 815–826 (2017).
- 835 69. Marks, E. *et al.* Oral Delivery of Prolyl Hydroxylase Inhibitor : AKB-4924 Promotes
836 Localized Mucosal Healing in a Mouse Model of Colitis. *Inflamm Bowel Dis* **21**,
837 267–275 (2015).
- 838 70. Li, X. *et al.* Therapeutic Potential of a Prolyl Hydroxylase Inhibitor FG-4592 for
839 Parkinson ' s Diseases in Vitro and in Vivo : Regulation of Redox Biology and
840 Mitochondrial Function. *Frontiers (Boulder)*. **10**, 1–16 (2018).
- 841 71. Rubtsov, Y. P. *et al.* Regulatory T Cell-Derived Interleukin-10 Limits Inflammation
842 at Environmental Interfaces. *Immunity* **28**, 546–558 (2008).
- 843 72. Kim, J. J., Shajib, S., Manocha, M. M. & Khan, W. I. Investigating Intestinal
844 Inflammation in DSS-induced Model of IBD. *Jove* **1**, 1–6 (2012).
- 845 73. Radu, M. & Chernoff, J. An in vivo assay to test blood vessel permeability. *J. Vis.*
846 *Exp.* 2–5 (2013).

848
849
850

851 **Acknowledgments**

852 We thank Valérie Acolty, Caroline Abdelaziz and Véronique Dissy for animal care and
853 for technical support. The development of mouse models of toxoplasmosis would not
854 have been possible without the kind assistance of Guillaume Oldenhove. This work was
855 supported by the European Regional Development Fund (ERDF) and the Walloon
856 Region (Wallonia-Biomed portfolio, 411132- 957270), a grant from the Fonds Jean
857 Brachet and research credit from the National Fund for Scientific Research, FNRS,
858 Belgium. FA is a Research Associate at the FNRS. YA is recipient of a research
859 fellowship from the FNRS/Télévie. HH has been supported by a Belgian FRIA
860 fellowship.

861

862 **Additional information**

863 The authors declare that the research was conducted in the absence of any commercial
864 or financial relationships that could be construed as a potential conflict of interest.

Figure legends

Figure 1. PHD2^{ΔTreg} mice display a spontaneous Th1-like inflammatory syndrome.

a Body weight of naive mice was determined weekly. **b** At 12 weeks of age, male and female mice were examined for rectal prolapse **c** splenomegaly and colon length summarized in **d**. **e** Representative gross autopsy of an hemorrhagic abdomen, (**f-i**) Lymphoid cells from spleen, mesenteric (mLN), peripheral (pLN) lymph nodes or the small intestine lamina propria were collected from Foxp3^{cre} and PHD2^{ΔTreg} mice. **f** Frequency of conventional, Foxp3⁻ CD4 and CD8-expressing cells among TCRβ-expressing T lymphocytes. **g** Representative merged (n = 15) t-distributed stochastic neighbor embedding (t-SNE) plot after dimensionality reduction and unsupervised clustering of flow cytometry data from CD4-expressing spleen cells. Relative distributions of CD4⁺ lymphocyte subsets are shown as doughnut charts. **h** Frequency of effector-like (CD44^{hi} CD62L^{lo}) conventional T lymphocytes in the indicated lymphoid organs. **i** Frequency of IFN-γ (top panel) and IL-17A (bottom panel) producing CD4⁺ T cells after in vitro stimulation. **j** Expression of inflammatory cytokines determined by qPCR on extracts from unfractionated mLNs. Data are representative of at least three independent experiments with n = 9 (**a, j**), n = 25 (**d**), n = 15 (**f-i**) per group. Values are presented as the mean ± standard deviation (SD) and were compared by two-tailed unpaired student's t-test. Only significant differences are indicated as follows: *: p<0.05, **: p<0.01, ***: p<0.001, ****: p<0.0001. Abbreviations: Naive Tconv (Foxp3⁻ CD44⁻ CD62L⁺), Memory Tconv (Foxp3⁻ CD44⁺ CD62L⁺), Effector Tconv (Foxp3⁻ CD44⁺ CD62L⁻), Memory Treg (Foxp3⁺ CD44⁺CD62L⁺), Effector Treg (Foxp3⁺ CD44⁺CD62L⁻).

865

866 Figure 2. Increased number, but altered phenotype of PHD2-deficient Treg cells.

867 Lymphoid cells from the thymus, spleen, mesenteric (mLN) and peripheral (pLN) lymph
868 nodes were collected at 12 weeks of age from Foxp3^{cre} and PHD2^{ΔTreg} male and female
869 mice and the relative frequency and phenotype of Foxp3-expressing cells were
870 established by flow cytometry or qPCR. **a** Frequency of Foxp3-expressing cells among
871 CD4-positive T lymphocytes; **b** Representative flow cytometry expression profiles of
872 Foxp3 and CD25 expression among thymic CD4⁺ T cells; **c** frequency of mature-like
873 (CD25⁺ Foxp3⁺) and Treg precursors subsets identified respectively as CD25⁻ Foxp3^{lo}
874 and CD25⁺ Foxp3⁻ cells among thymic CD4⁺ T cells; **d** frequency of immature-like,
875 CD24⁺ Foxp3⁺ T cells in the thymus of adult mice; **e** frequency of effector (CD62L^{low}
876 CD44^{high}), memory (CD62L^{high} CD44^{high}) and naive (CD62L^{high} CD44^{low}) splenic Foxp3-
877 expressing cells; **f** frequency of splenic Tregs expressing the master transcription
878 factors T-bet, GATA3 and RORγt; **g** Ratio of the Foxp3 MFI of PHD2-KO splenic Tregs
879 to Foxp3^{cre} splenic Tregs. **h** Expression of CD25, CD44, ICOS, PD-1 and CTLA-4 in
880 splenic Treg of Foxp3^{cre} and PHD2^{ΔTreg} mice. Top panel, representative traces of MFI.
881 Bottom panel, ratios of the MFIs of PHD2-KO Treg to Foxp3^{cre} Treg cells are expressed
882 as the mean ± SD. **i** *Il10* gene expression relative to RPL32 by ex-vivo purified Tregs
883 was determined by qPCR. (**j-i**) CD4⁺ Foxp3⁻ splenic naive T cells were stimulated in

884 vitro with anti-CD3/CD28 (5/1 $\mu\text{g ml}^{-1}$) in the presence of TGF- β (3 $\mu\text{g ml}^{-1}$) and IL-2 (10
885 $\mu\text{g ml}^{-1}$) for 72h to induce Treg polarization.

886 **j** Representative flow cytometry expression profiles of Foxp3 expression at the end of
887 the culture period. The first panel represents a typical profile of cells activated in the
888 absence of polarizing cytokines; **k** number of Foxp3⁺ cells generated in the culture
889 conditions; **l** Expression (MFI) of Foxp3 by in vitro induced Treg cells. Data are
890 representative of at least two independent experiments with n = 15 (**a, e-g**), n = 9 (**h, i**)
891 or n = 6 (**c, d, k, l**) per group. Values are presented as the mean \pm SD and were
892 compared by two-tailed unpaired student's t-test. Only significant differences are
893 indicated as follows: *: p<0.05, **: p<0.01, ***: p<0.001.

894

895 **Figure 3. Cell autonomous role of PHD2 in determining Treg cells phenotype.**

896 Spleen, thymus, mesenteric (mLN) and peripheral (pLN) lymph nodes were collected at
897 8 weeks of age from *Foxp3^{cre/+} EglN1^{fl/fl}* heterozygous female mice and the relative
898 frequency and phenotype of Foxp3-expressing cells were established by flow cytometry.

899 **a** Proportion of WT (YFP- cells) or PHD2-KO (YFP+ cells) Treg cells among Foxp3-
900 expressing cells. **b** representative histograms of Foxp3, CD25, CD44 and CTLA-4
901 expression in splenic WT Tregs (black lines) compared to splenic PHD2-KO Tregs (red
902 lines). **c** Foxp3 MFI, **d** CD25 MFI, **e** CD44 MFI and **f** CTLA-4 MFI of WT and PHD2-KO
903 Tregs in lymphoid organs. Data are representative of two independent experiments with
904 n = 9 per group. Values are presented as the mean \pm standard deviation (SD) and were
905 compared by two-tailed unpaired student's t-test. Only significant differences are
906 indicated as follows: *: p<0.05, **: p<0.01, ***: p<0.001, ****: p<0.0001.

907

Figure 4. Reduced in vivo but not in vitro suppressive capacity of PHD2-deficient Treg.

a Treg function was assayed following adoptive co-transfer of CD45.2 Foxp3-
expressing cells with naive, CFSE labeled congenic CD45.1 CD4⁺ lymphocytes (Treg :
Tconv ratio 1:3) into syngeneic lymphopenic male mice (*Rag2^{-/-}*). Recipient mice were
euthanized at day 6 post-transfer, and their spleen and mLN cells analyzed by flow
cytometry. **b** Representative flow cytometry expression profiles of CFSE labeled cells
(CD45.1 gate in the spleen) with or without co-transferred Foxp3⁺ cells from Foxp3^{cre} or
PHD2 Δ^{Treg} male mice; **c** percentage of suppression established from CFSE staining
profiles; **d** frequency of activated (CD4⁺ CD45.1⁺ CD44^{hi} CD62L^{lo}) cells in the indicated
lymphoid organs; **e** frequency of Treg cells in the indicated organs 6 days post-transfer.
(**f, g**) CFSE-labeled, naive conventional CD4⁺ T cells from CD54.1 mice were co-
cultured with ex-vivo purified Treg cells from Foxp3^{cre} or PHD2 Δ^{Treg} mice at the indicated
ratios in the presence of anti-CD3 antibodies (0.5 $\mu\text{g ml}^{-1}$) and splenic feeder cells; **f**
representative flow cytometry profiles of CSFE staining; **g** Percent of suppression of
proliferation as compared to cultures in which Treg cells were omitted. Data are
representative of three independent experiments with n = 15 (**b-e**) or n = 4 (**f, g**) per
group. Values are presented as the mean \pm SD and were compared by two-way
ANOVA with Tukey's multiple comparisons test (**c-e**) or by two-tailed unpaired student's
t-test (**g**). Only significant differences are indicated as follows: *: p<0.05, **: p<0.01, ***:
p<0.001.

Figure 5. Increased sensitivity of PHD2^{ΔTreg} mice to DSS-induced colitis and toxoplasmosis.

Foxp3^{cre} and PHD2^{ΔTreg} male mice were provided with 2% DSS in tap water for five days. On day 5, the 2% DSS water was replaced with normal drinking water and mice were followed during 14 days for **a** body weight, **b** survival, **c** colitis severity and **d** colon length. **e** Colons were isolated from untreated mice or 6 days after colitis induction and were fixed and stained with hematoxylin and eosin (H&E); arrows indicate inflammatory cell infiltrates. **f** Foxp3^{cre} and PHD2^{ΔTreg} male mice were infected by intragastric gavage with 10 cysts of ME-49 type II *Toxoplasma gondii* (control group are Foxp3^{cre} mice without treatment) and subsequently followed for **g** body weight. **h** Mice were sacrificed 8 days after infection to assess colon length; **i** frequency of effector-like (CD44^{hi} CD62L^{lo}) conventional T lymphocytes in the indicated lymphoid organs; **j** frequency of IFN-γ producing CD4⁺ T cells after in vitro stimulation; **k** frequency of T-bet⁺ among Foxp3⁺(Treg) cells. Data are representative of three independent experiments with n = 20 (**a, b**), n = 10-14 (**c, d**), n = 5 (**e**) or n = 10 (**g-k**) per group. Values are presented as the mean ± SD and were compared by two-tailed unpaired student's t-test (**a, c, g**), by Mantel-Cox test (**b**), by one-way ANOVA with Tukey's multiple comparisons test (**d, h**) or by two-way ANOVA with Tukey's multiple comparisons test (**i-k**). Only significant differences are indicated as follows: *: p<0.05, **: p<0.01, ***: p<0.001, ****: p<0.0001.

Figure 6. Concomitant loss of HIF2α but not HIF1α expression attenuates the proinflammatory phenotype of PHD2^{ΔTreg} mice.

a Representative gross autopsy of spleens and colon length summarized in **b** of Foxp3^{cre}, PHD2^{ΔTreg}, PHD2-HIF1α^{ΔTreg}, PHD2-HIF2α^{ΔTreg} and PHD2-HIF1α-HIF2α^{ΔTreg} (TKO) mice. **c** Representative merged (n = 15) t-distributed stochastic neighbor embedding (t-SNE) plot after dimensionality reduction and unsupervised clustering of flow cytometry data from CD4-expressing spleen cells. Relative distributions of CD4⁺ lymphocyte subsets are shown as doughnut charts. (**d-g**) Lymphoid cells from spleen, mesenteric (mLN), peripheral (pLN) lymph nodes or the small intestine lamina propria were collected from Foxp3^{cre}, PHD2^{ΔTreg}, PHD2-HIF1α^{ΔTreg} mice, PHD2-HIF2α^{ΔTreg} and PHD2-HIF1α-HIF2α^{ΔTreg} (TKO) male and female mice and the relative frequency and phenotype of Foxp3-positive and Foxp3-negative, conventional T lymphocytes determined by flow cytometry. **d** Frequency of effector-like (CD44^{hi} CD62L^{lo}) conventional T lymphocytes in the indicated lymphoid organs. **e** Frequency of IFN-γ producing CD4⁺ T cells after in vitro stimulation. **f** Frequency of Foxp3-expressing cells among CD4-positive T lymphocytes. **g** Ratio of the Foxp3 MFI of PHD2-KO, PHD2-HIF1αKO, PHD2-HIF2αKO or TKO splenic Tregs to Foxp3^{cre} splenic Tregs. Data are representative of at least three independent experiments with n = 15 per groups. Values are expressed as the mean ± SD and were compared by One-way ANOVA with Tukey's multiple comparisons test (**b, g**) or by Two-way ANOVA with Tukey's multiple comparisons test (**d-f**). Only significant differences are indicated as follows: *: p<0.05, **: p<0.01, ***: p<0.001, ****: p<0.0001.

908 **Figure 7. Anti-inflammatory response, response to chemokines and cell survival**
909 **pathways represent targets of the PHD2-HIF2 α axis in Tregs.**

910 Splenic Treg cells were purified by cell sorting from Foxp3^{cre} (n = 3), PHD2 ^{Δ Treg} (n = 2),
911 PHD2-HIF1 α ^{Δ Treg} (n = 2), PHD2-HIF2 α ^{Δ Treg} (n = 3) and PHD2-HIF1 α -HIF2 α ^{Δ Treg} (TKO) (n
912 = 3) male mice and total RNA was extracted and sequenced by RNA-sequencing
913 (Illumina). **a** Heatmap of genes differentially expressed. Values are represented as Log₂
914 fold-change obtained from median of each gene and are plotted in red-blue color scale
915 with red indicating increased expression and blue indicating decreased expression.
916 Hierarchical clustering of genes (k mean clustering) show 20 clusters. **b** Classification of
917 mouse strains according to their spontaneous inflammation severity. **c** Heatmap of
918 genes downregulated when PHD2 and PHD2-HIF1 α are deleted and whose expression
919 is restored to a control level (close to Foxp3^{cre} Treg) following deletion of HIF2 α (Cluster
920 10, 181 genes). **d** Heatmap of genes upregulated when PHD2 and PHD2-HIF1 α are
921 deleted and whose expression is restored to a control level following deletion of HIF2 α
922 (Cluster 11, 66 genes). **e** Heatmap of genes upregulated when PHD2 and PHD2-HIF2 α
923 are deleted and whose expression is restored to a control level following deletion of
924 HIF1 α (Cluster 3, 98 genes). Cluster 3, 10 and 11 were subjected to functional
925 annotations and regulatory network analysis in the Ingenuity Pathway Analysis (IPA)
926 software. Data were analyzed using Deseq2, a gene is differentially expressed when
927 Log₂FC (Fold change) > 0.5 and FDR (False discovery rate) <0.05.

928

929 **Figure 8. Identification of STAT1-mediated signaling as a target of the PHD2-**
930 **HIF2 α axis in Tregs.**

931 **a** Upregulated and downregulated genes (cluster 10 and 11 in **Figure 6 c-d**) were
932 imported into the Ingenuity Pathway Analysis (IPA) software and were subjected to
933 Upstream regulator analysis (URA) prediction algorithms. STAT1 was predicted as an
934 upstream regulators of downregulated genes with a p-value = 3.10^{-12} . Phosphorylated
935 form of STAT1 (pSTAT1 (Tyr701)) was assessed by flow cytometry after brief in vitro
936 stimulation (30 min) of splenic CD4⁺ T lymphocytes with recombinant IFN- γ . **b**
937 Representative histogram of pSTAT1 MFI for conventional CD4⁺ T cells (Tconv) and
938 Treg cells of Foxp3^{cre}, PHD2 ^{Δ Treg} and PHD2-HIF2 α ^{Δ Treg} male mice. Mean value
939 expression (represented by MFI) of **c** pSTAT1 or **d** STAT1 total protein by splenic Treg
940 of Foxp3^{cre}, PHD2 ^{Δ Treg} and PHD2-HIF2 α ^{Δ Treg} mice. **e** Frequency of Treg cells expressing
941 the CXCR3 receptor. Data are representative of three independent experiments with n =
942 9 (**b-d**) or n = 12 (**e**) per groups. Values are presented as the mean \pm SD and were
943 compared by one-way ANOVA with Tukey's multiple comparisons. Only significant
944 differences are indicated as follows: **: p<0.01, ***: p<0.001.

Figure supplement legends

Figure 1-figure supplement 1. Treg-restricted loss of *Egln1* gene expression in PHD2^{ΔTreg} mice.

a Treg cells from Foxp3^{cre} male and female mice were purified by cell sorting from spleen (n = 10), mesenteric (mLN) (n = 8), peripheral (pLN) lymph nodes (n = 4) or the small intestine lamina propria (n = 4) and expression of *Egln2* (PHD1), *Egln1* (PHD2) and *Egln3* (PHD3) analyzed by qPCR. **b** YFP-positive (YFP⁺) and YFP-negative (YFP⁻) cells from PHD2-sufficient (Foxp3^{cre} mice) and PHD2-deficient (PHD2^{ΔTreg} mice) were purified by cell sorting from spleen and mesenteric lymph nodes (mLN) and expression of *Egln1* analyzed by qPCR. The graph demonstrates selective loss of *Egln1* gene expression in Tregs, but not in Tconvs purified from PHD2^{ΔTreg} mice. **c** *lfng* gene expression relative to RPL32 by ex-vivo purified Tregs from spleen and mLN was determined by qPCR. **d** Representative flow cytometry expression profile of GLUT1, a specific HIF1α target gene in Foxp3 expressing or non-expressing cells from Foxp3^{cre} and PHD2^{ΔTreg} mice. **e** Frequency of GLUT1-expressing Tregs in lymphoid organs from Foxp3^{cre} and PHD2^{ΔTreg} mice. Data are representative of two independent experiments with n = 6 per group. Values are presented as the mean ± SD and were compared by two-tailed unpaired student's t-test. Only significant differences are indicated as follows: *: p<0.05, **: p<0.01, ***: p<0.001, ****: p<0.0001.

Figure 1-figure supplement 2. Increased blood cells counts and elevated hematocrit in PHD2^{ΔTreg} mice associated with an increase in vascular permeability.

a White blood cell (WBC) counts, **b** red blood cell (RBC) counts, **c** platelet (PLT) counts and **d** hematocrit (HCT) from Foxp3^{cre}, PHD2^{ΔTreg} and PHD2-HIF2α^{ΔTreg} male mouse blood. To assess vascular permeability mice were i.v injected with a 0,5% Blue Evans (BE) solution, and the indicated, organs collected after 30 minutes and placed in formamide at 55°C during 24 hours. The absorbance of supernatants was measured at 600 nm, **e** representative image of the colon supernatant after 24h in formamide, **f** ng of Blue Evans per mg of tissue for spleen, mesenteric lymph nodes (mLN), colon and liver of different groups of mice injected or not with Blue Evans. Data are representative of two (a-d) or three (e-f) independent experiments with n = 7-9 per group (a-d) or n = 4-6 per group (e-f). Values are presented as the mean ± standard deviation (SD) and were compared by one-way ANOVA (a-d) or two-way ANOVA (f) with Tukey's multiple comparisons test. Only significant differences are indicated as follows: *: p<0.05, **: p<0.01, ***: p<0.001, ****: p<0.0001.

Figure 1-figure supplement 3. Gating strategy for flow cytometry data analysis.

Representative flow cytometry dot plots displaying the gating strategy for the identification of conventional T cell populations in Figures 1, 3, 4 and 5 and for identification of regulatory T cell subsets in Figures 2, 4 and 8

Figure 1-figure supplement 4. Absolute cell counts.

Absolute cell counts of **a** CD4⁺ T cells, **b** CD8⁺ T cells, **c** regulatory T cells and **d** activated conventional T cells in the spleen, mesenteric (mLN), peripheral (pLN) lymph

nodes and the small intestine lamina propria of Foxp3^{cre} and PHD2^{ΔTreg} male and female mice. Data are representative of at least three independent experiments with, n = 15 per group. Values are presented as the mean ± standard deviation (SD) and were compared by two-tailed unpaired student's t-test. Only significant differences are indicated as follows: *: p<0.05, **: p<0.01, ***: p<0.001, ****: p<0.0001.

Figure 5-figure supplement 1. PHD2^{ΔTreg} mice display a near-normal response to anti-CD3-induced enteritis.

Foxp3^{cre} and PHD2^{ΔTreg} female mice were injected twice i.p. with anti-CD3 mAbs (20μg) at two days interval and weighted daily. **a** Weight loss was found similar in both mouse strains tested; **b** relative expression of inflammatory mediators evaluated by qPCR on whole, unfractionated mesenteric lymph nodes. A similar, Th17-like response was observed in both mouse strains. Data are representative of two independent experiments with n = 6 per group. Values are presented as the mean ± SD and were compared by one-way ANOVA with Tukey's multiple comparisons test. Only significant differences are indicated as follows: *: p<0.05, **: p<0.01.

Figure 5-figure supplement 2. Loss of *Ifng* gene expression attenuates the pro-inflammatory phenotype of PHD2^{ΔTreg} mice

PHD2^{ΔTreg} mice were crossed with IFN-γKO mice (PHD2^{ΔTreg} IFN-γ^{KO} mice) and were compared to Foxp3^{cre} and PHD2^{ΔTreg} male and female mice and analyzed for **a** colon length; **b** frequency of effector-like (CD44^{hi} CD62L^{lo}) conventional T lymphocytes in the indicated lymphoid organs; **c** frequency of IFN-γ production after in vitro stimulation; **d** frequency of IL-17A-producing cells after in vitro stimulation and **e** frequency of Foxp3⁺ cells in the indicated lymphoid organs. Data are representative of three independent experiments with n = 10 per groups. Values are expressed as the mean ± SD and were compared by One-way ANOVA with Tukey's multiple comparisons test (**a**) or by Two-way ANOVA with Tukey's multiple comparisons test (**b-e**). Only significant differences are indicated as follows: *: p<0.05, **: p<0.01, ***: p<0.001, ****: p<0.0001.

Figure 6-figure supplement 1. Treg-selective HIF1α or HIF2α deficiency does not affect immune homeostasis in naive mice.

a Splenic Treg cells were purified by cell sorting from Foxp3^{cre} (n = 3), PHD2^{ΔTreg} (n = 2), PHD2-HIF1α^{ΔTreg} (n = 2), PHD2-HIF2α^{ΔTreg} (n = 3), PHD2-HIF1α-HIF2α^{ΔTreg} (TKO) (n = 3), HIF1α^{ΔTreg} (n = 3) and HIF2α^{ΔTreg} (n = 3) male mice and their genotype verified by qPCR on the extracted total RNA fraction. **b** representative gross autopsy findings revealing normal spleen and colon size (summarized in panel **c**) in 12 weeks aged male and female mice. **d** frequency of CD4⁺ Foxp3⁻ CD44^{hi} CD62L^{lo} cells in lymphoid organs; **e** frequency of CD4⁺ lymphocytes producing IFN-γ upon in vitro stimulation; **f** frequency of Foxp3⁺ cells in the indicated lymphoid organs; **g** Ratio of the Foxp3 MFI of HIF1αKO or HIF2αKO splenic Tregs to Foxp3^{cre} splenic Tregs. Data are representative of three independent experiments with n = 10. Values are presented as the mean ± SD and were compared by one-way ANOVA with Tukey's multiple comparisons test (**c**, **g**) or by Two-way ANOVA with Tukey's multiple comparisons test (**d-f**). No statistical difference were found between groups.

Figure 7-figure supplement 1. Signaling pathways affected by loss of PHD2-expression in Treg.

a Top significantly downregulated pathways in PHD2-deficient Tregs compared to Tregs from Foxp3^{cre} mice **b** top significantly upregulated pathways in PHD2-deficient Tregs compared to Tregs from Foxp3^{cre} mice. Affected pathways were determined by over representation analysis (ORA analysis) in R program after Deseq2 analysis. Dots color and size represent respectively FDR (false discovery rate) and the number of genes affected in a given pathway.

Figure 8-figure supplement 1. Gating strategy for identification of YFP⁺ cells.

Representative flow cytometry dot plots displaying the gating strategy for the identification of YFP positive populations in the: **a** spleen, **b** mLN, **c** thymus and **d** liver. Although the majority of YFP-expressing cells also expressed Foxp3, a minor population (from 1 to 3% depending on the organ considered) of YFP cells lacked expression of both CD45 and Foxp3, suggesting a possible expression of the Cre-recombinase in non-hematopoietic cells in PHD2^{ΔTreg} mice.

Source data files

Figure 1- source data 1

Figure 2- source data 1

Figure 3- source data 1

Figure 4- source data 1

Figure 5- source data 1

Figure 6- source data 1

Figure 7- source data 1

Figure 8- source data 1

Figure 1-figure supplement 1- source data 1

Figure 1-figure supplement 2- source data 1

Figure 1-figure supplement 4- source data 1

Figure 5-figure supplement 1- source data 1

Figure 5-figure supplement 2- source data 1

Figure 6-figure supplement 1- source data 1

Figure 7-figure supplement 1- source data 1

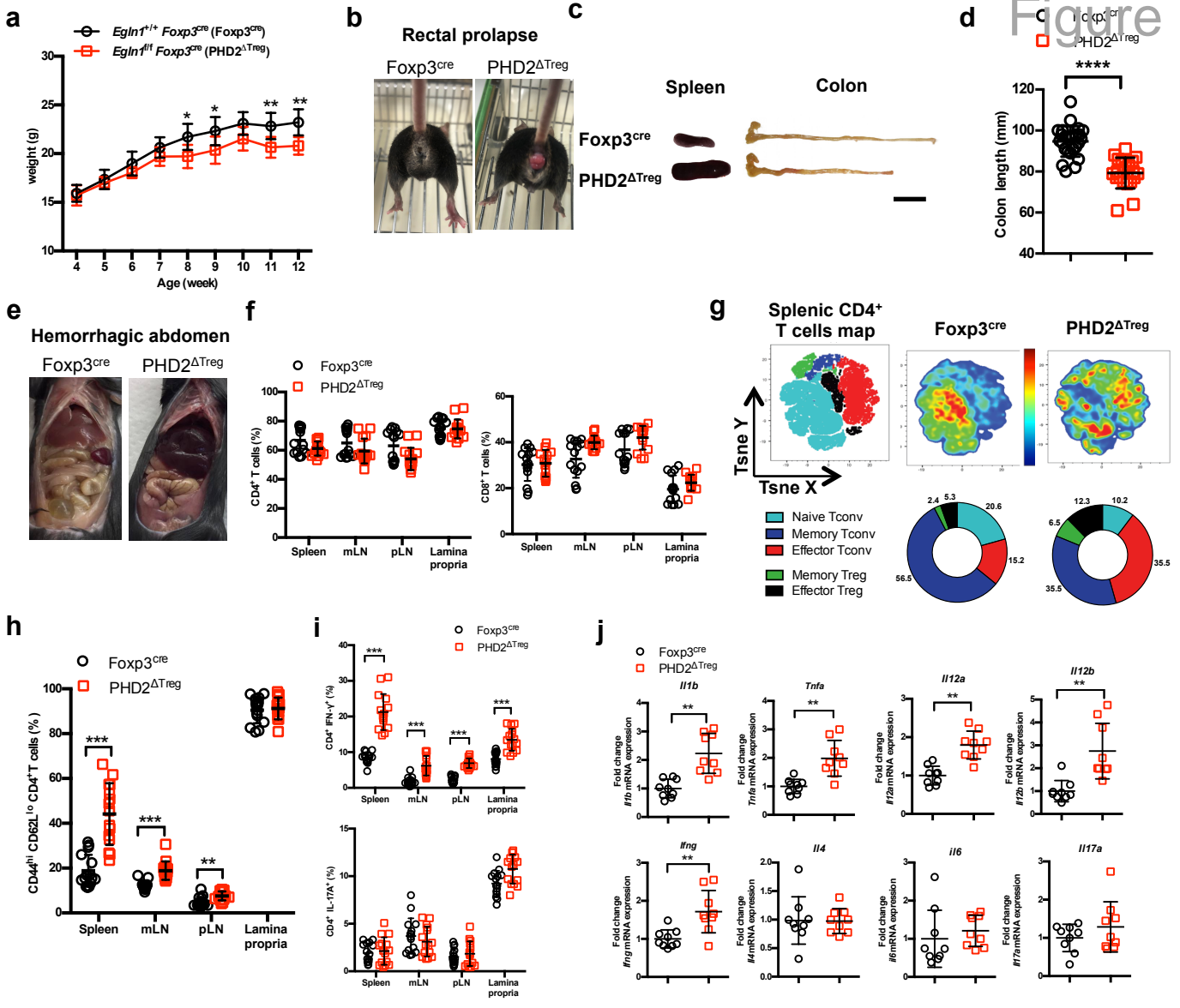


Figure 1. PHD2^{ΔTreg} mice display a spontaneous Th1-like inflammatory syndrome.

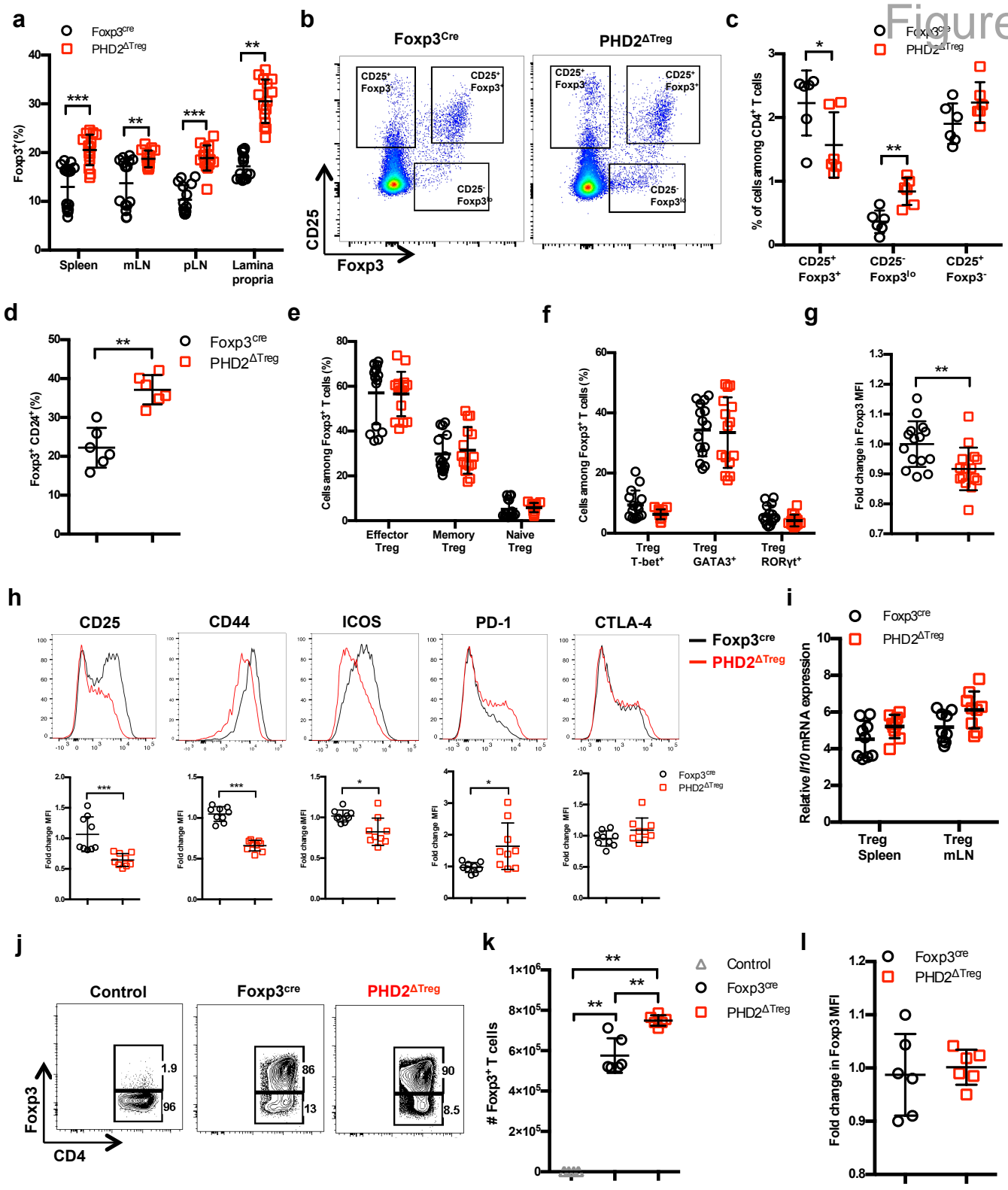


Figure 2. Increased number, but altered phenotype of PHD2-deficient Treg cells.

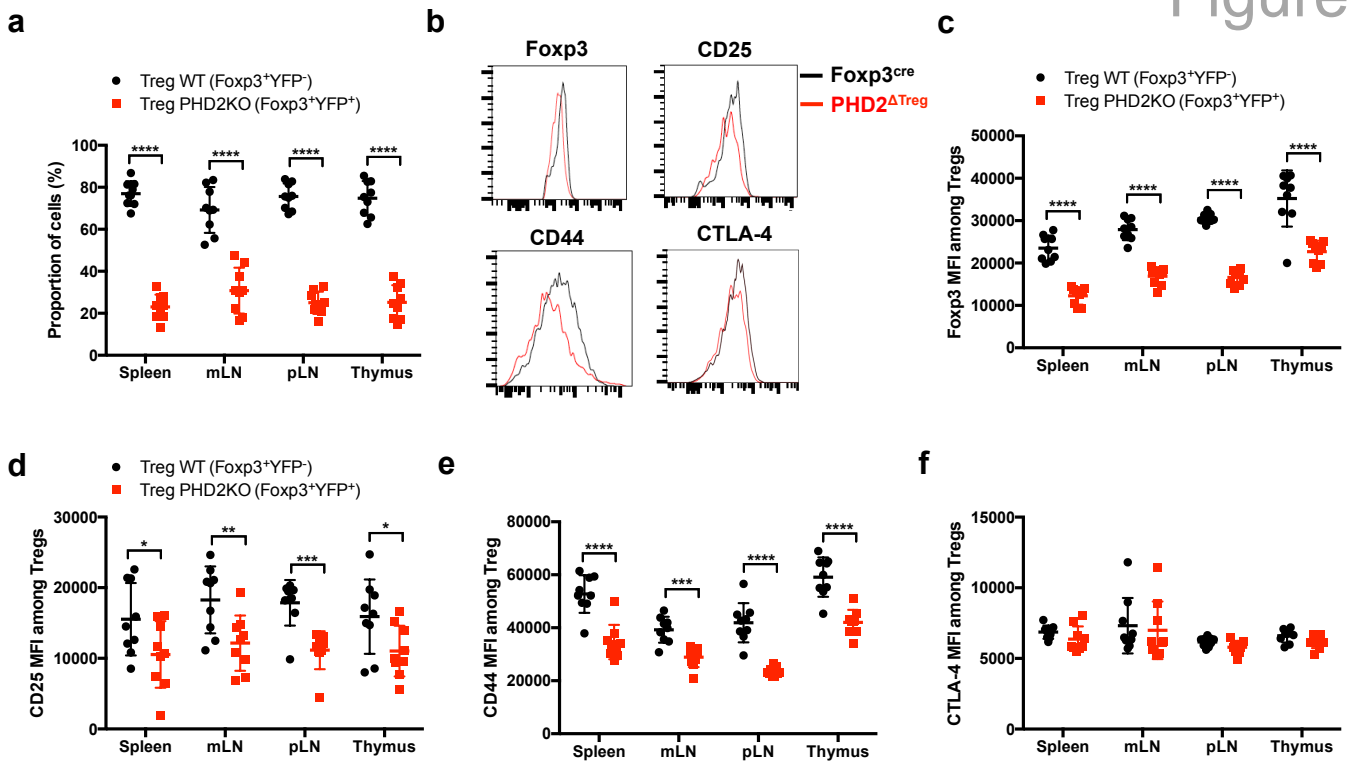


Figure 3. Cell autonomous role of PHD2 in determining Treg cells phenotype.

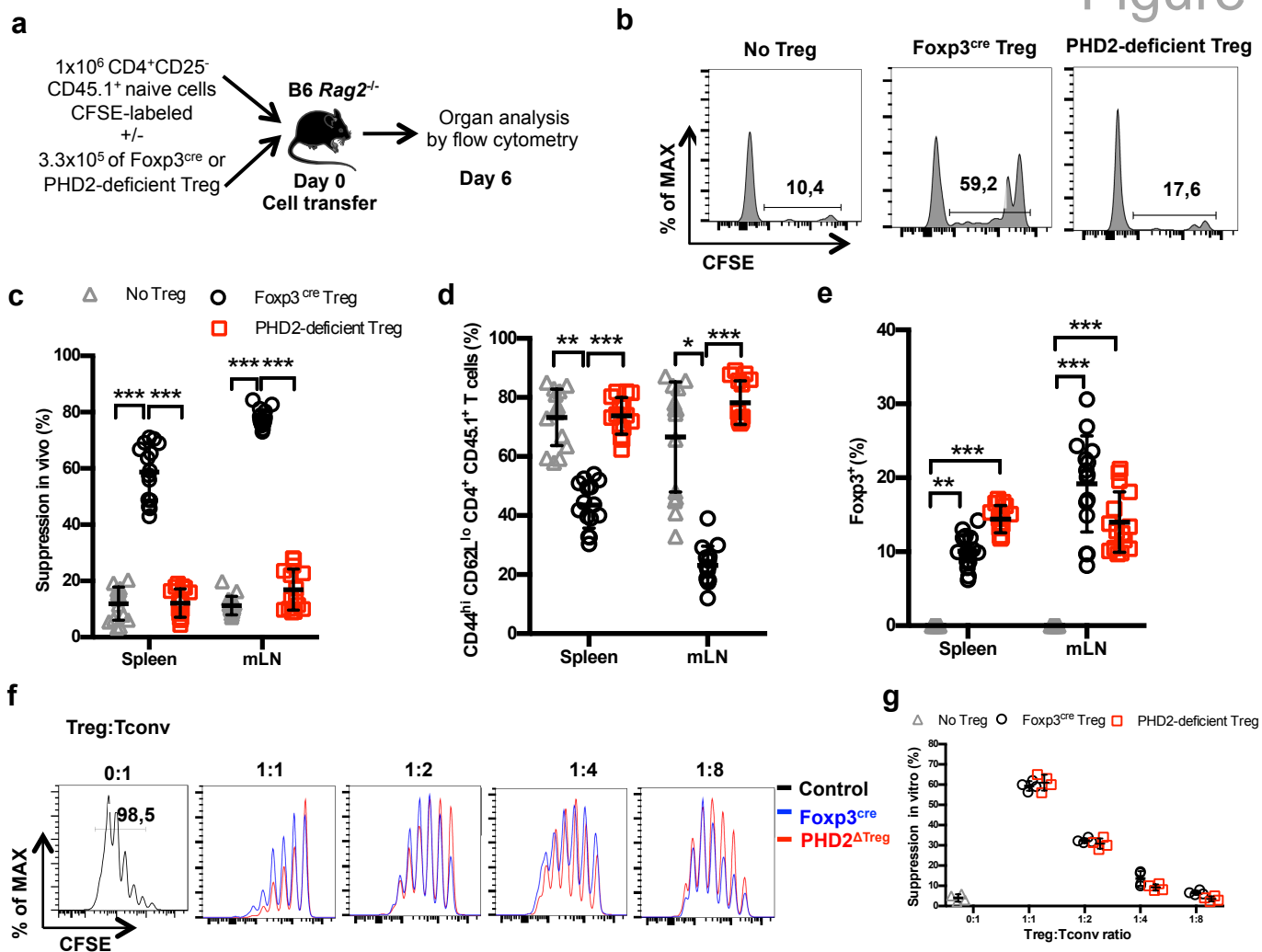


Figure 4. Reduced in vivo but not in vitro suppressive capacity of PHD2-deficient Treg.

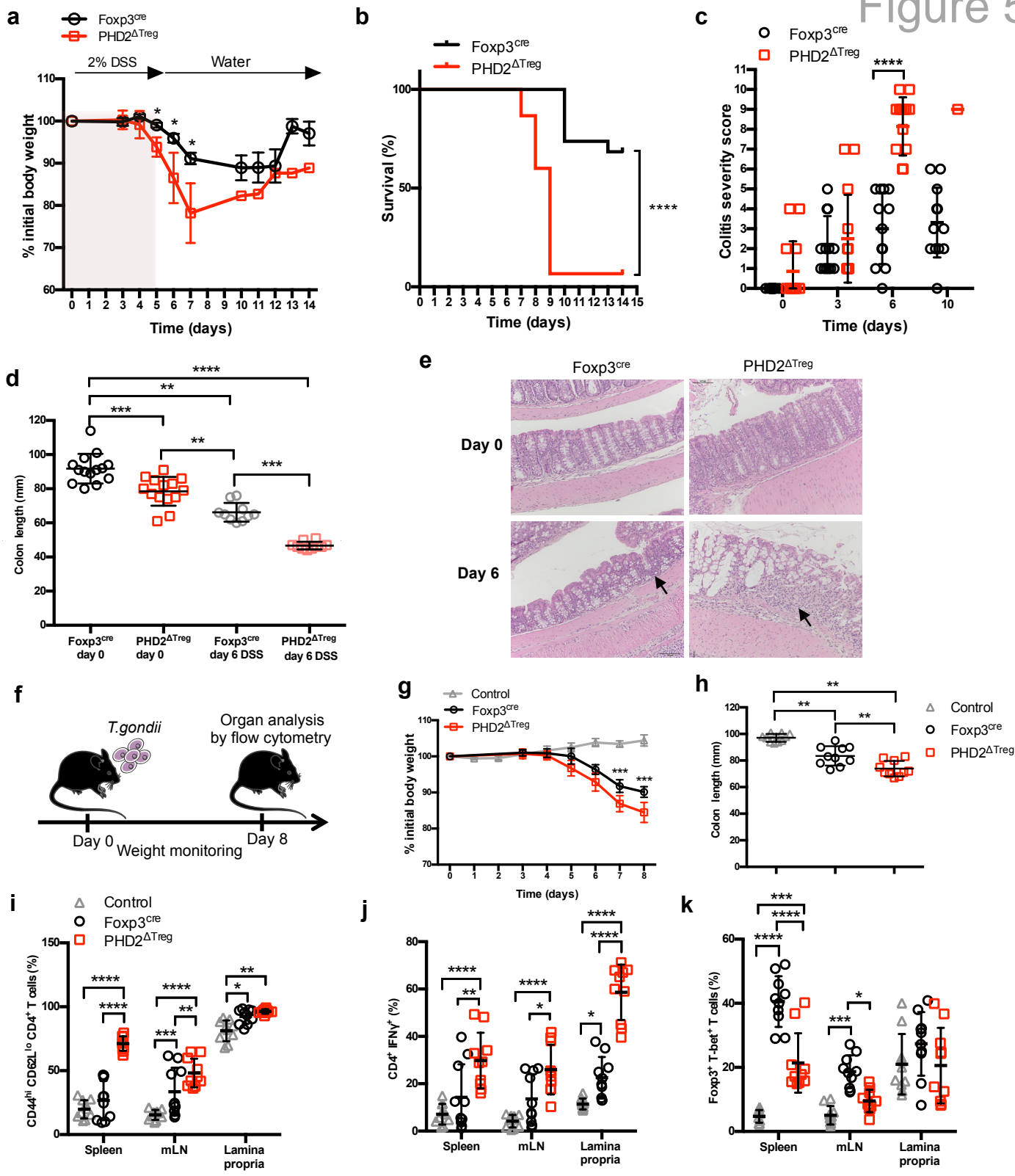


Figure 5. Increased sensitivity of PHD2^{ΔTreg} mice to DSS-induced colitis and toxoplasmosis.

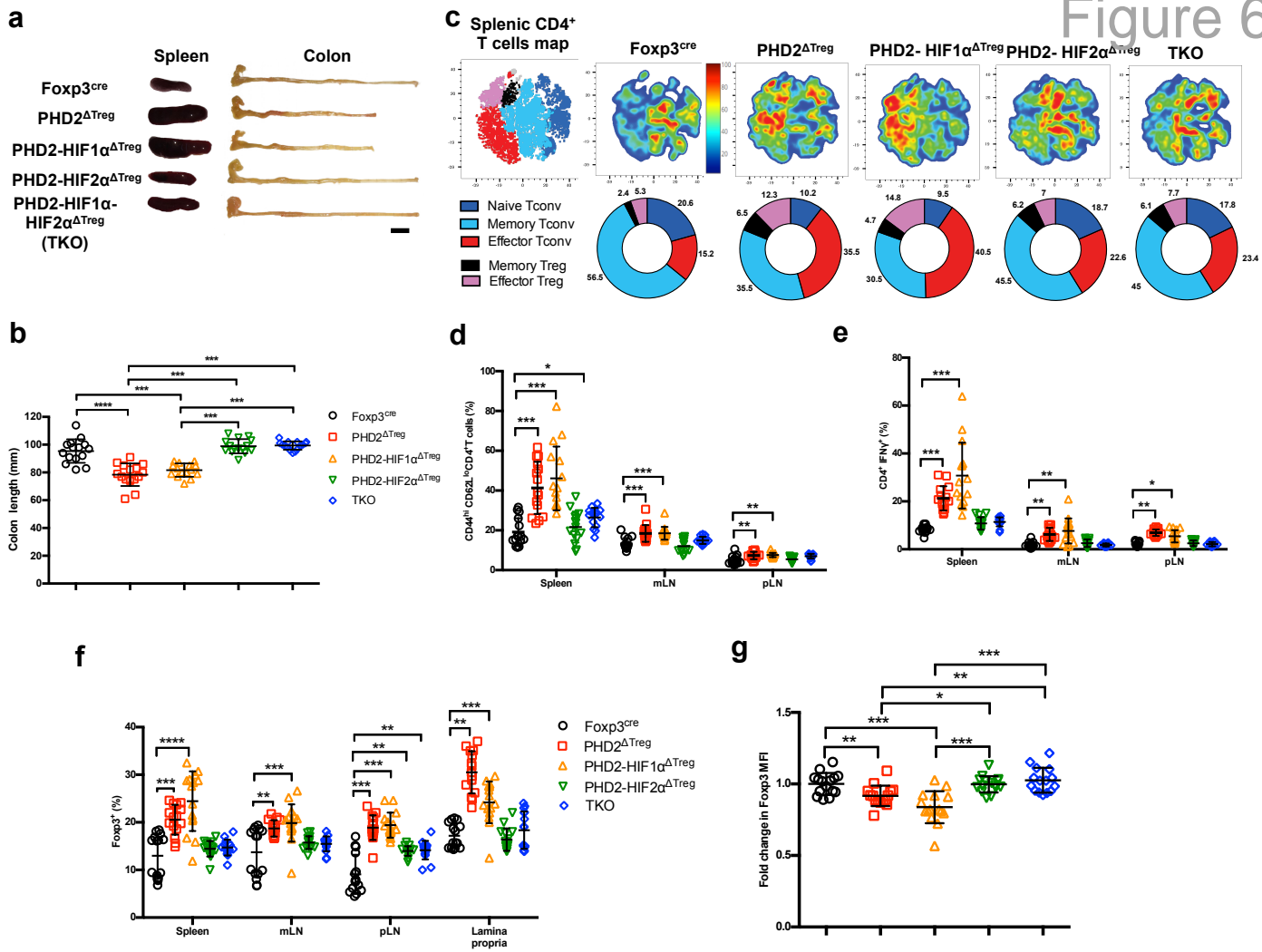


Figure 6. Concomitant loss of HIF2 α but not HIF1 α expression attenuates the proinflammatory phenotype of PHD2 Δ Treg mice.

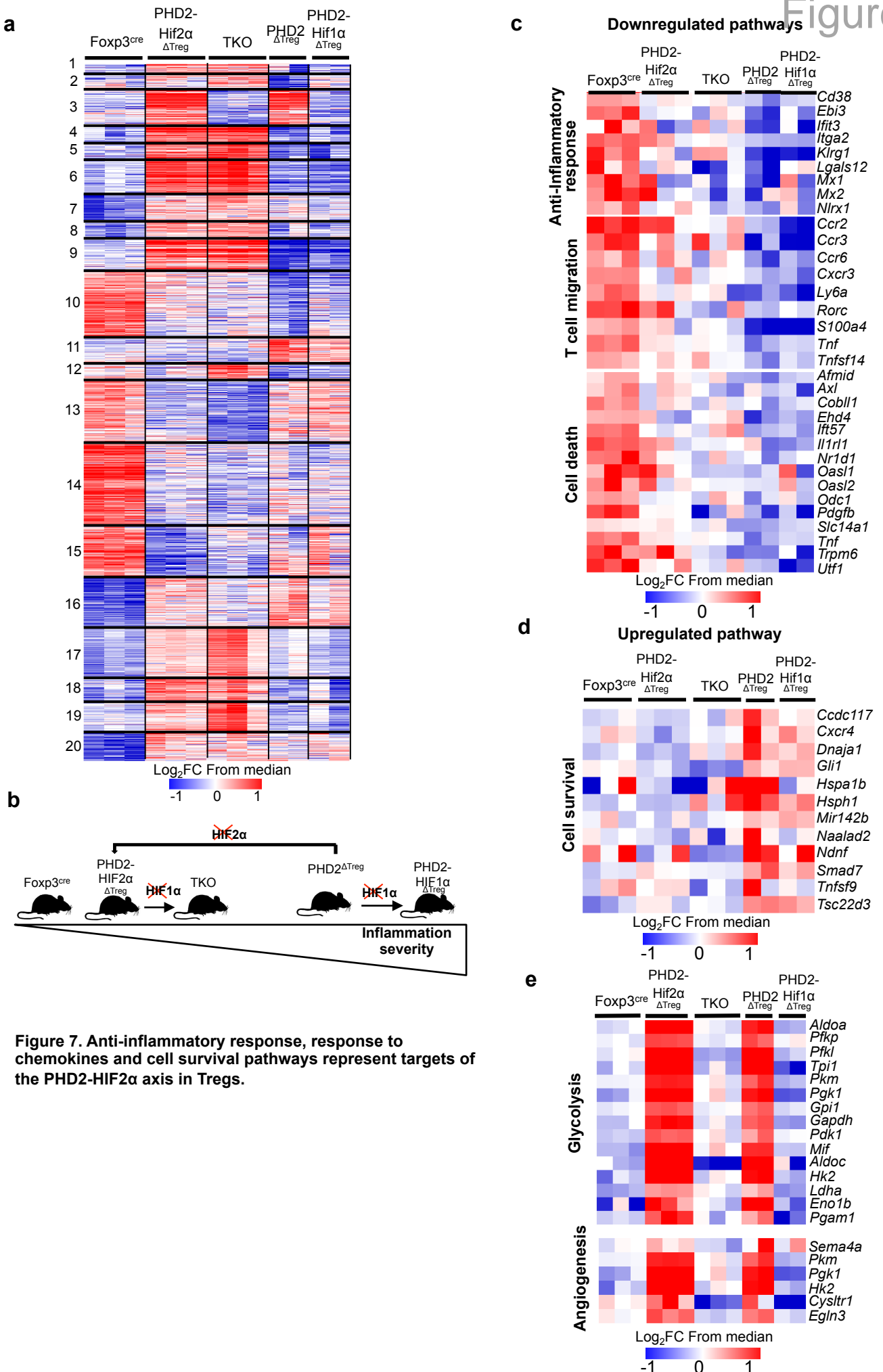


Figure 7. Anti-inflammatory response, response to chemokines and cell survival pathways represent targets of the PHD2-HIF2 α axis in Tregs.

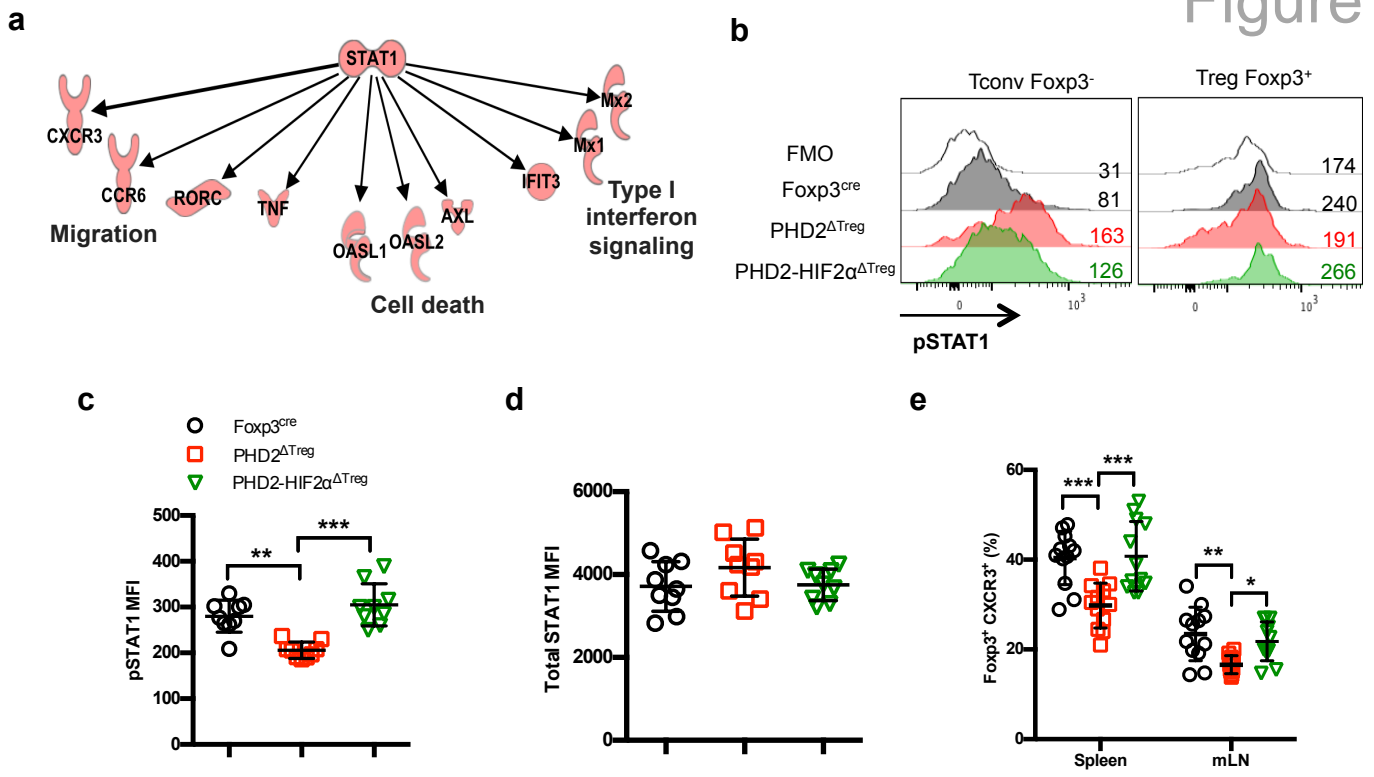


Figure 8. Identification of STAT1-mediated signaling as a target of the PHD2-HIF2 α axis in Tregs.

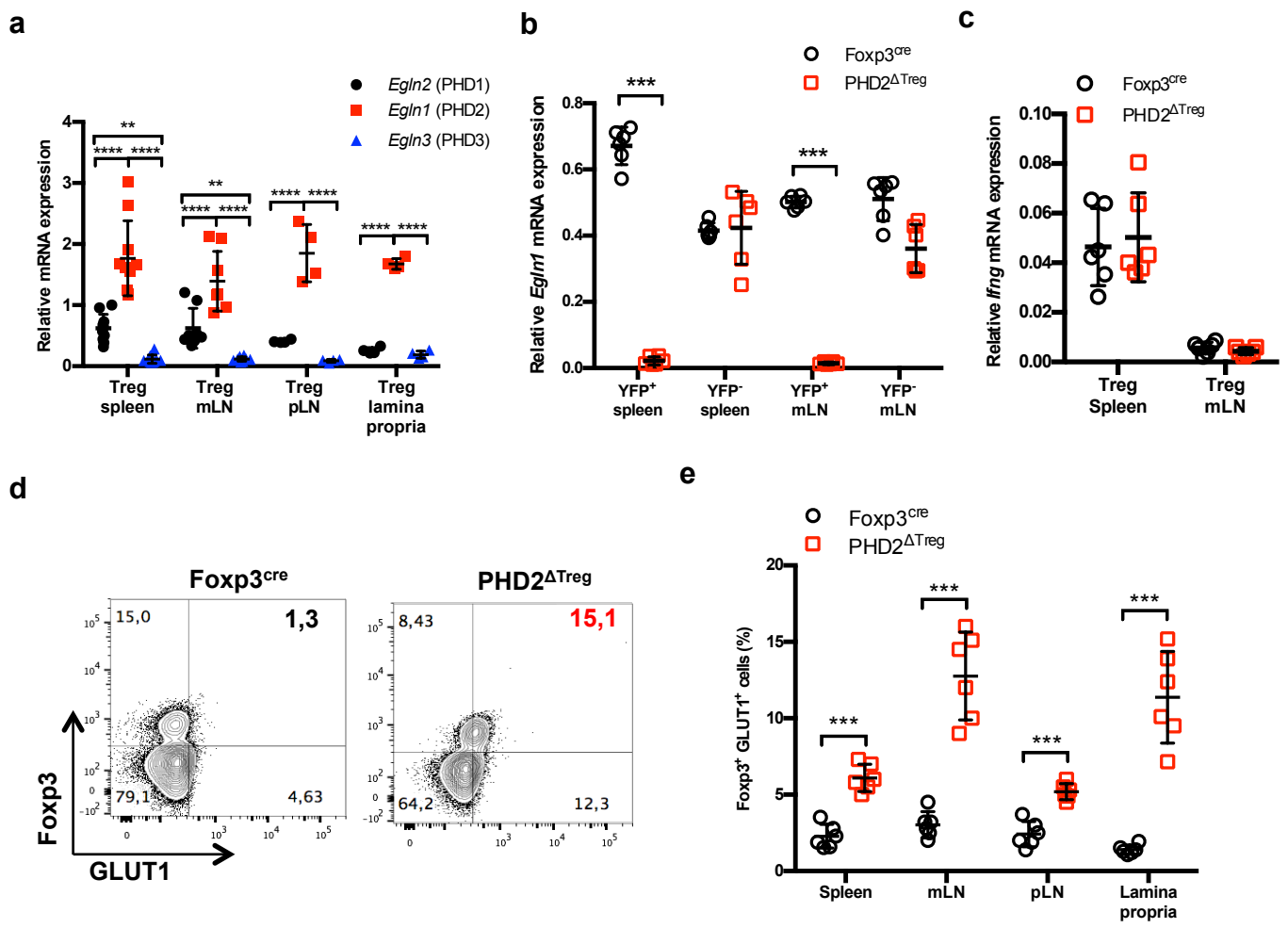


Figure 1-figure supplement 1. Treg-restricted loss of *Egl1* gene expression in *PHD2*^{ΔTreg} mice.

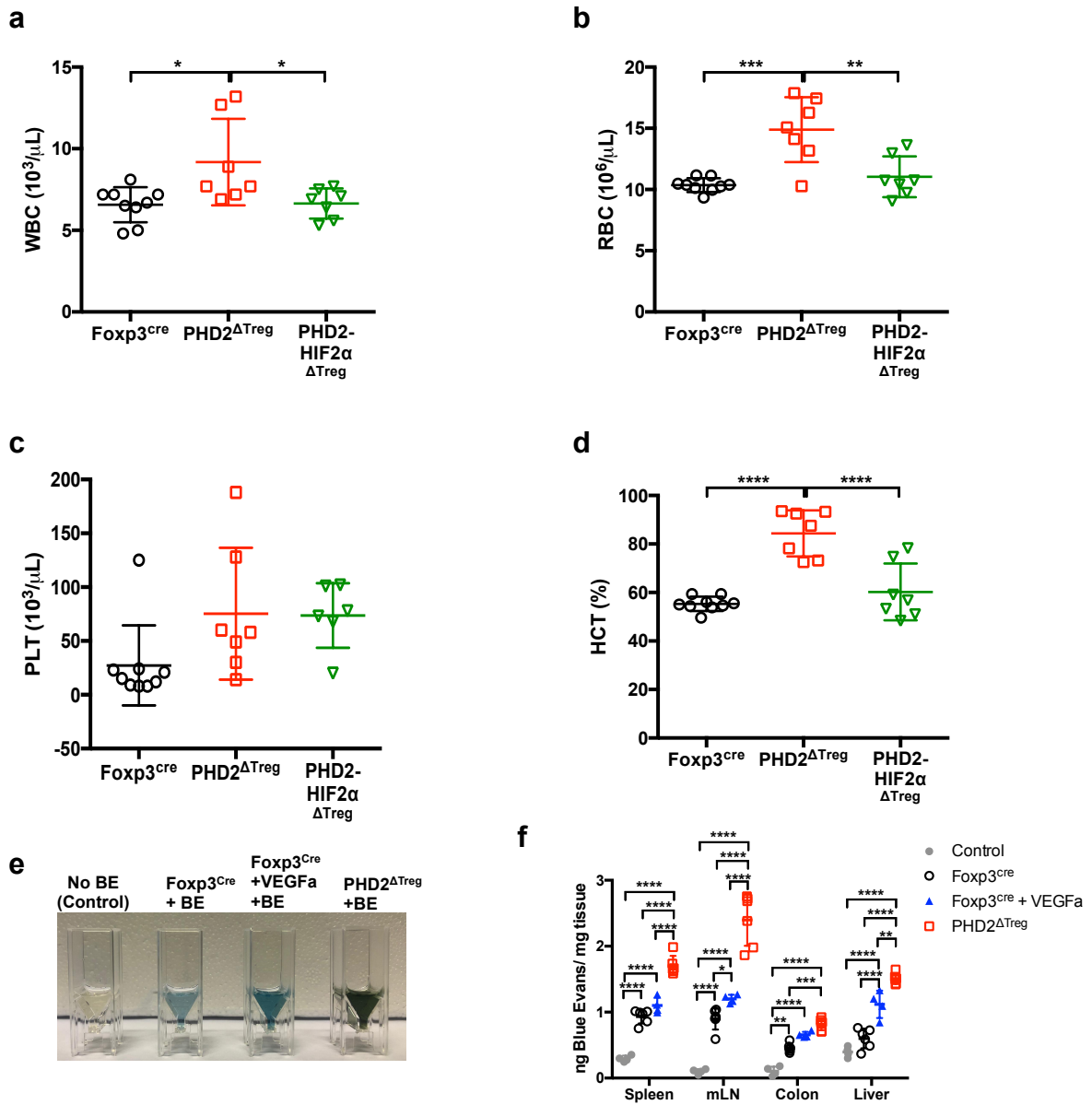


Figure 1-figure supplement 2. Increased blood cells counts and elevated hematocrit in PHD2^{ΔTreg} mice associated with an increase in vascular permeability.

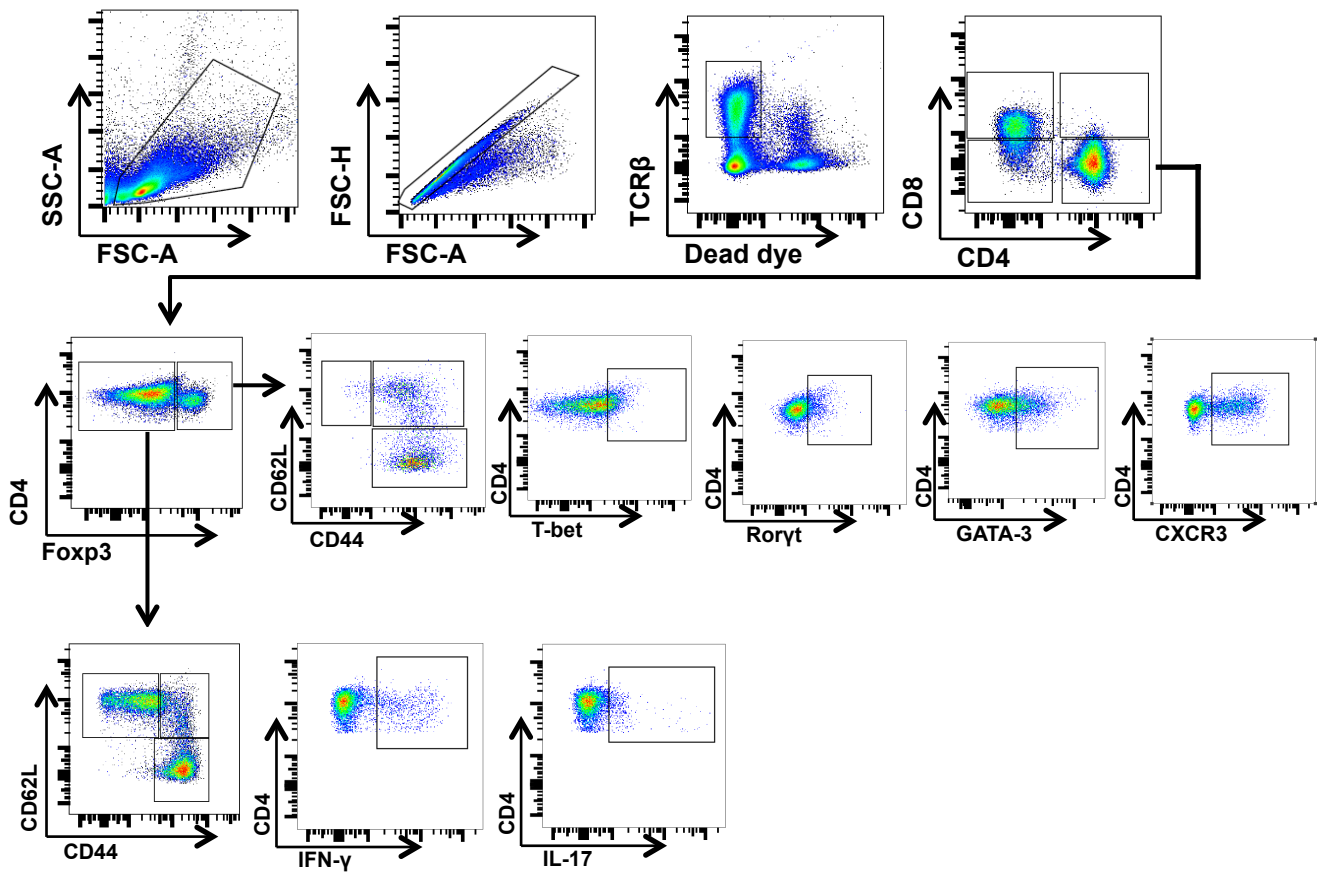


Figure 1-figure supplement 3. Gating strategy for flow cytometry data analysis.

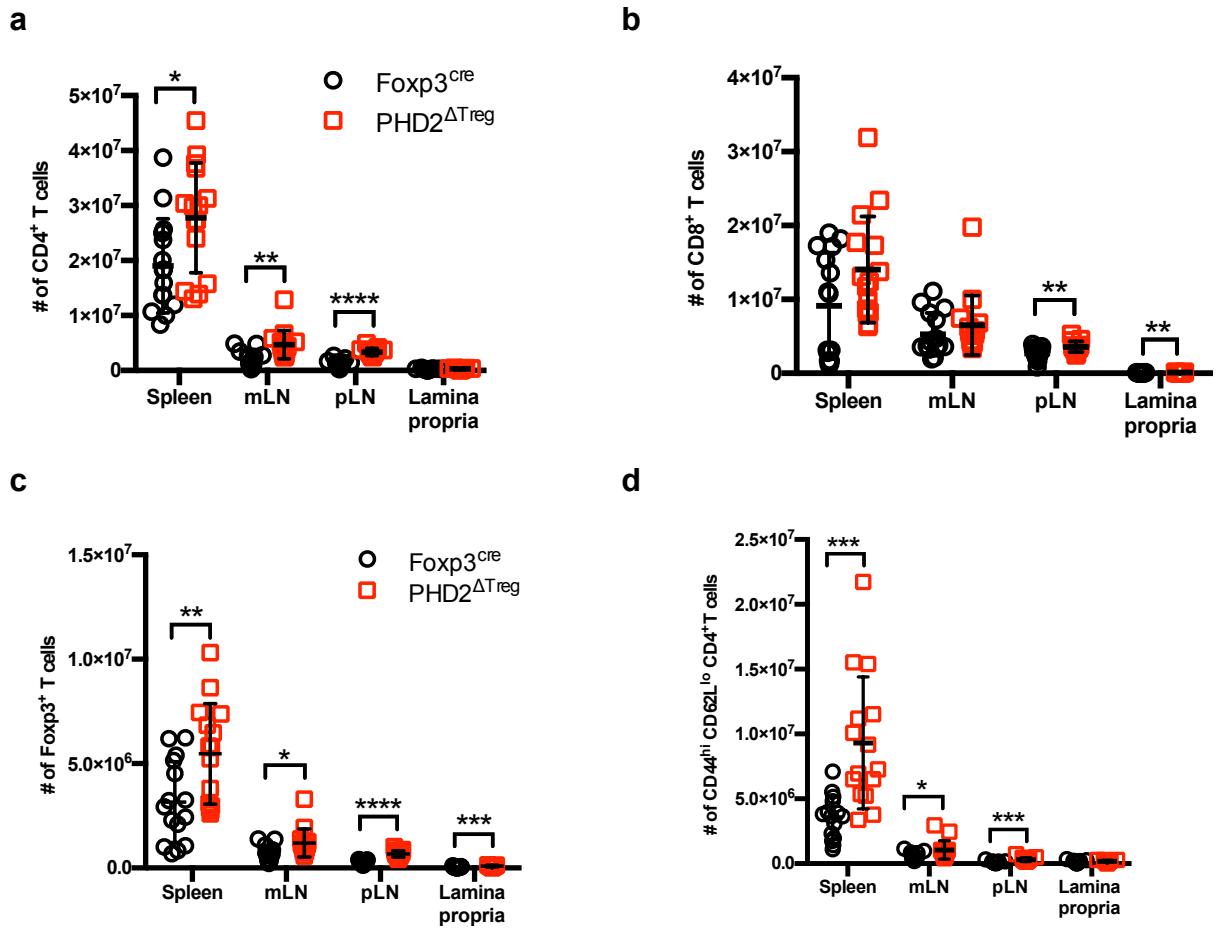


Figure 1-figure supplement 4. Absolute cell counts.

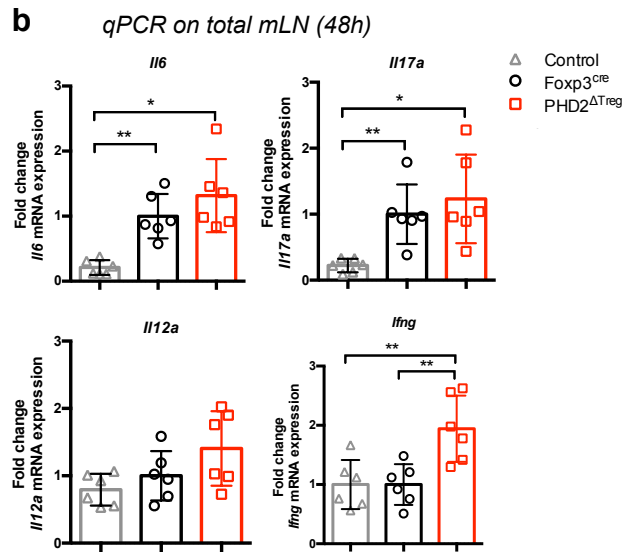
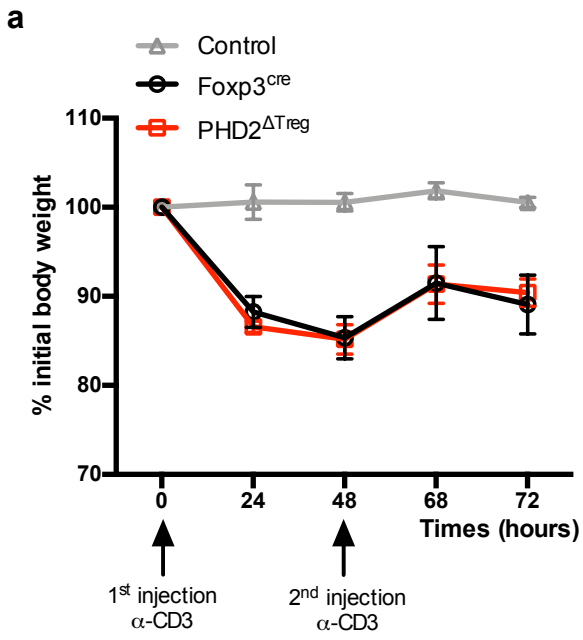


Figure 5-figure supplement 1. PHD2^{ΔTreg} mice display a near-normal response to anti-CD3-induced enteritis.

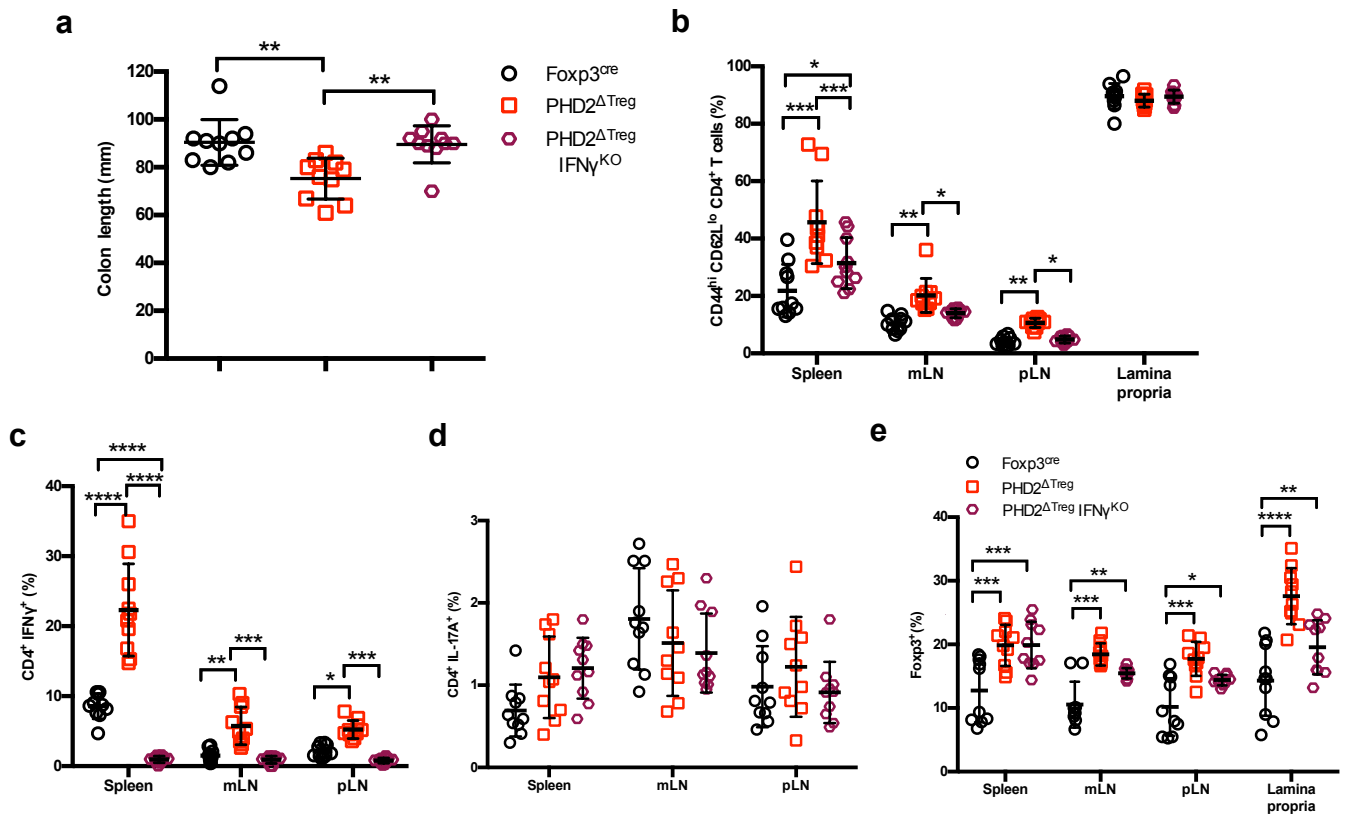


Figure 5-figure supplement 2. Loss of *Ifng* gene expression attenuates the pro-inflammatory phenotype of PHD2 Δ Treg mice

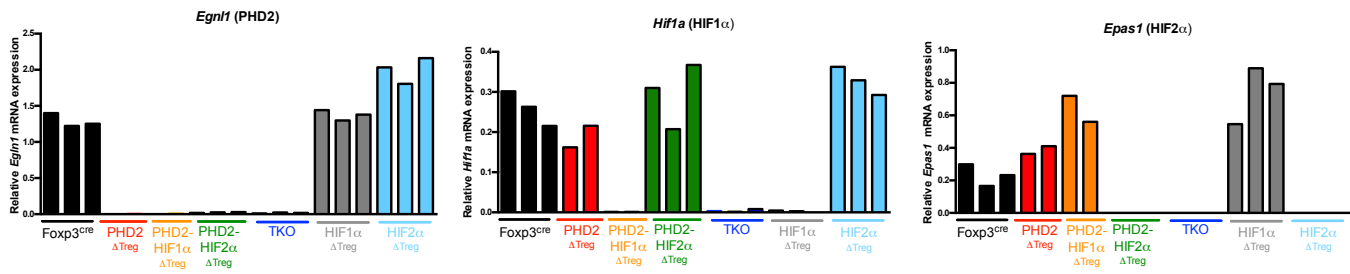
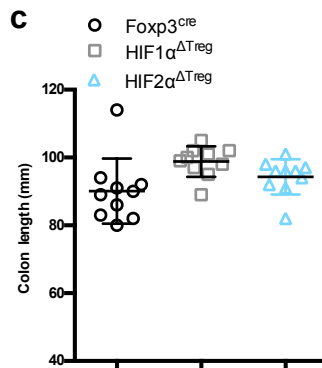
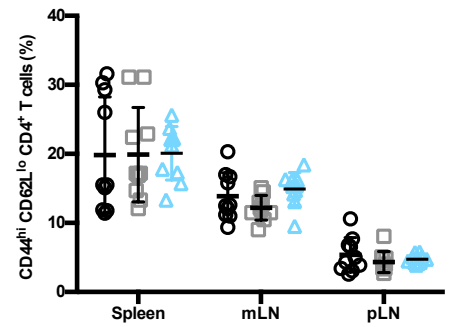
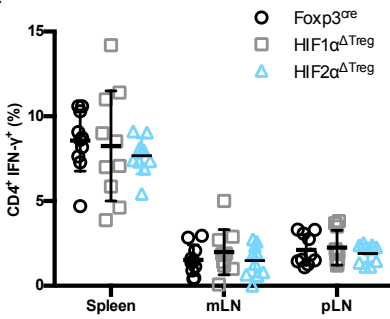
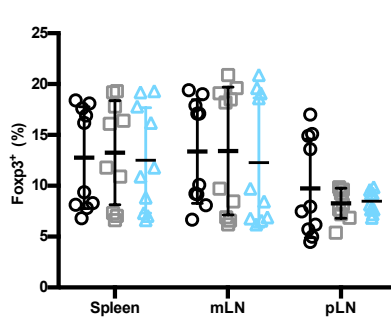
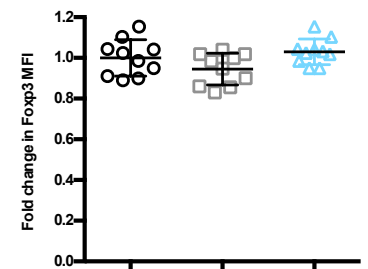
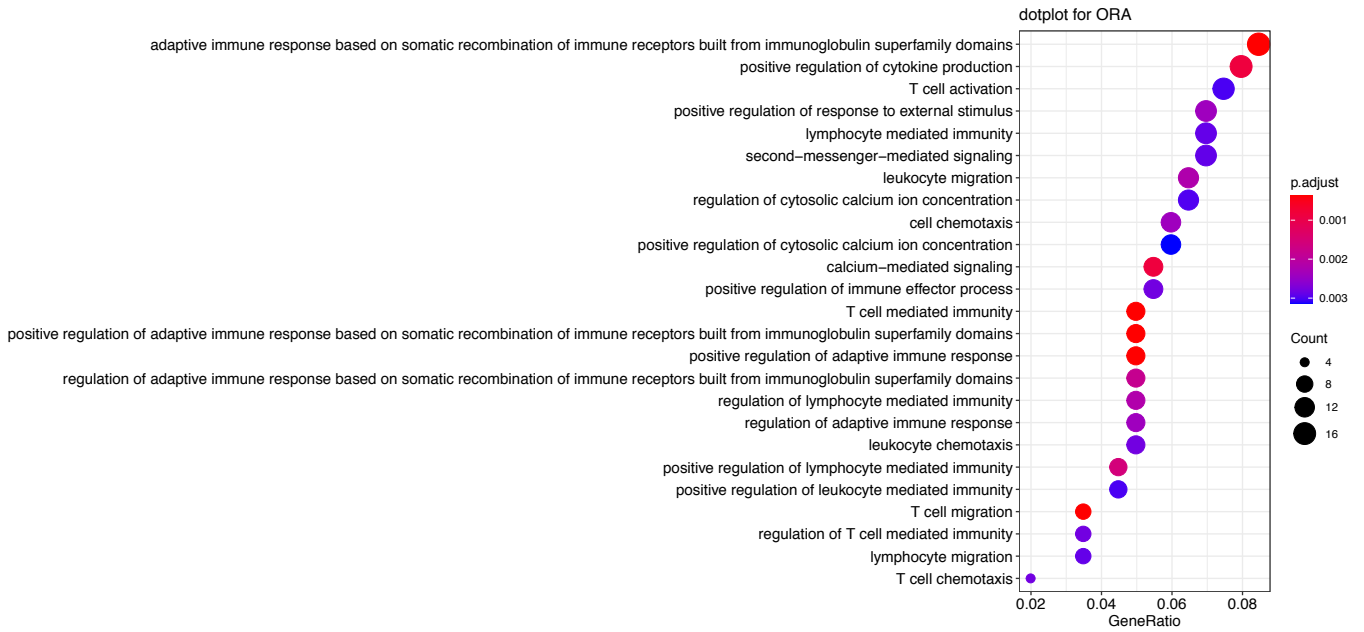
a**b****c****d****e****f****g**

Figure 6-figure supplement 1. Treg-selective HIF1 α or HIF2 α deficiency does not affect immune homeostasis in naive mice.

a Downregulated pathways



b Upregulated pathways

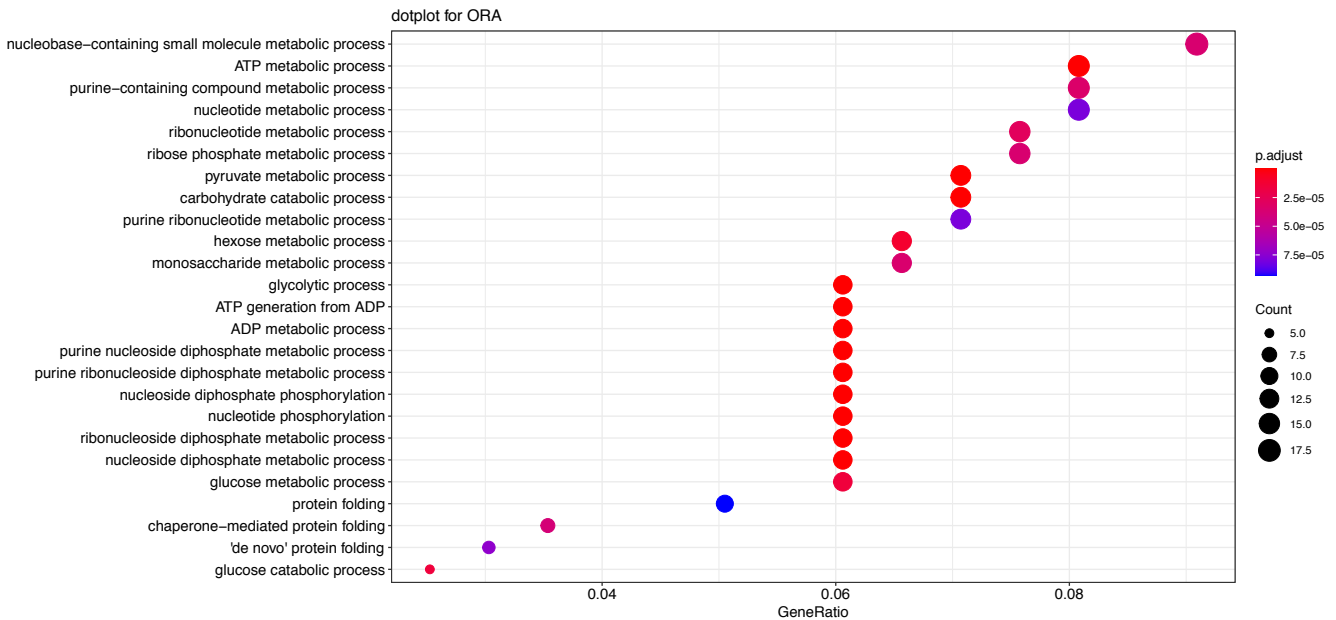


Figure 7-figure supplement 1. Signaling pathways affected by loss of PHD2-expression in Treg.

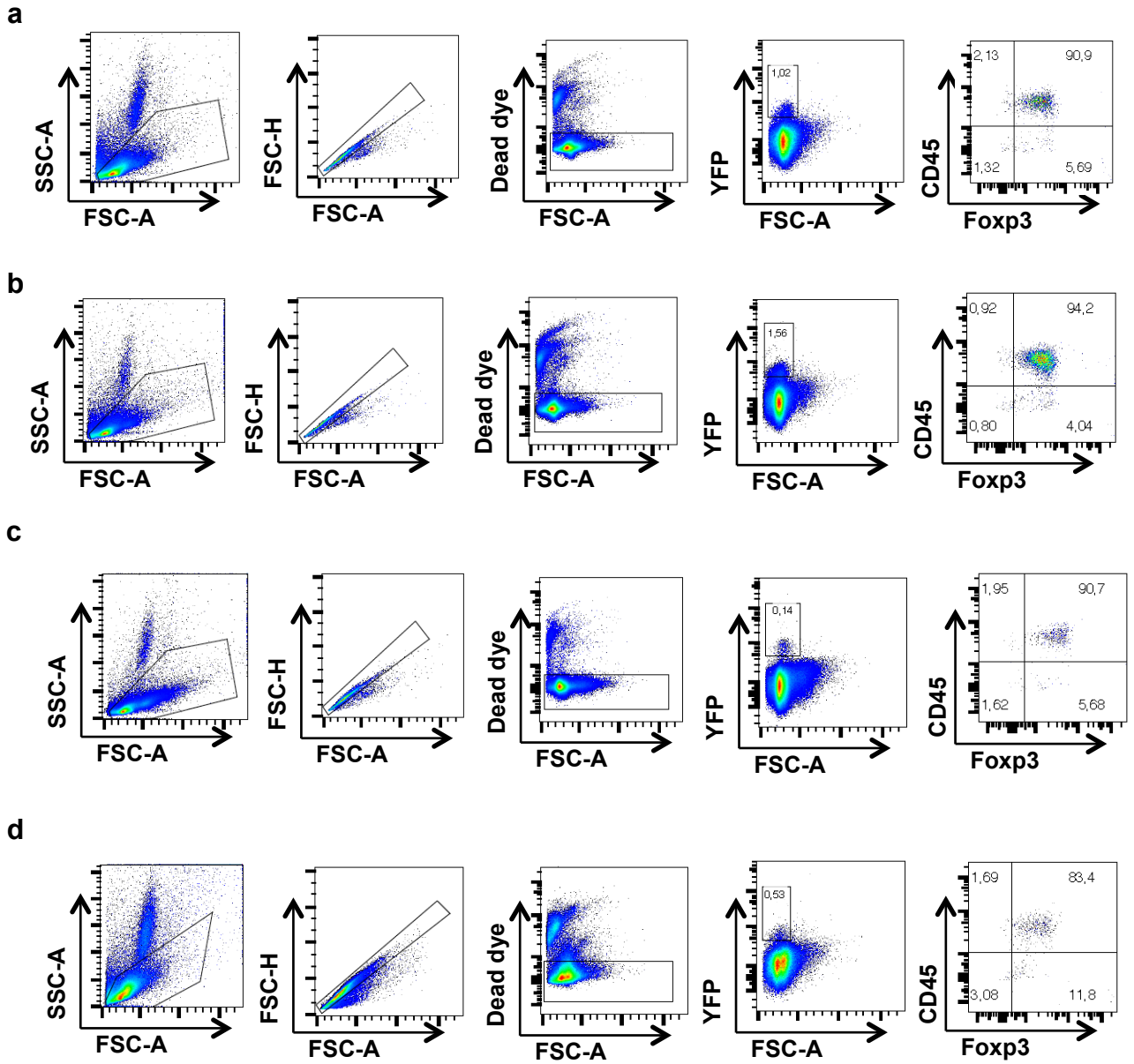


Figure 8-figure supplement 1. Gating strategy for identification of YFP⁺ cells.